



Article

Ring Opening Polymerization of Lactides and Lactones by Multimetallic Titanium Complexes Derived from the Acids $\text{Ph}_2\text{C}(\text{X})\text{CO}_2\text{H}$ ($\text{X} = \text{OH}, \text{NH}_2$)

Xin Zhang ¹, Timothy J. Prior ¹, Kai Chen ², Orlando Santoro ^{1,3} and Carl Redshaw ^{1,*}¹ Plastics Collaboratory, Department of Chemistry, University of Hull, Cottingham Road, Hull HU6 7RX, UK² Collaborative Innovation Center of Atmospheric Environment and Equipment Technology, Jiangsu Key Laboratory of Atmospheric Environment Monitoring and Pollution Control, School of Environmental Science and Engineering, Nanjing University of Information Science & Technology, Nanjing 210044, China³ Dipartimento di Biotecnologie e Scienze della Vita, Università degli Studi dell'Insubria, 21100 Varese, Italy

* Correspondence: c.redshaw@hull.ac.uk

Abstract: The reactions of the titanium alkoxide $[\text{Ti}(\text{OR})_4]$ ($\text{R} = \text{Me}, n\text{Pr}, i\text{Pr}, t\text{Bu}$) with the acids $2,2'\text{-Ph}_2\text{C}(\text{X})(\text{CO}_2\text{H})$, where $\text{X} = \text{OH}$ and NH_2 , i.e., benzoic acid ($2,2'$ -diphenylglycolic acid, L^1H_2), and $2,2'$ -diphenylglycine (L^2H_3), have been investigated. The variation of the reaction stoichiometry allows for the isolation of mono-, bi-, tri or tetra-metallic products, the structures of which have been determined by X-ray crystallography. The ability of the resulting complexes to act as catalysts for the ring opening polymerization (ROP) of ϵ -caprolactone (ϵ -CL) and *r*-lactide (*r*-LA) has been investigated. In the case of ϵ -CL, all catalysts except that derived from $[\text{Ti}(\text{O}n\text{Pr})_4]$ and L^2H_3 , i.e., **7**, exhibited an induction period of between 60 and 285 min, with **7** exhibiting the best performance (>99% conversion within 6 min). The PCL products are moderate- to high-molecular weight polymers. For *r*-LA, systems **1**, **3**, **4** and **7** afforded conversions of ca. 90% or more, with **4** exhibiting the fastest kinetics. The molecular weights for the PLA are somewhat higher than those of the PCL, with both cyclic and linear PLA products (end groups of OR/OH) identified. Comparative studies versus the $[\text{Ti}(\text{OR})_4]$ starting materials were conducted, and although high conversions were achieved, the control was poor.

Keywords: titanium complexes; benzoic acid; $2,2'$ -diphenylglycine; molecular structures; ring opening polymerization; ϵ -CL; *r*-LA



Citation: Zhang, X.; Prior, T.J.; Chen, K.; Santoro, O.; Redshaw, C. Ring Opening Polymerization of Lactides and Lactones by Multimetallic Titanium Complexes Derived from the Acids $\text{Ph}_2\text{C}(\text{X})\text{CO}_2\text{H}$ ($\text{X} = \text{OH}, \text{NH}_2$). *Catalysts* **2022**, *12*, 935. <https://doi.org/10.3390/catal12090935>

Academic Editor: Ruairaidh McIntosh

Received: 5 August 2022

Accepted: 19 August 2022

Published: 24 August 2022

Publisher's Note: MDPI stays neutral with regard to jurisdictional claims in published maps and institutional affiliations.

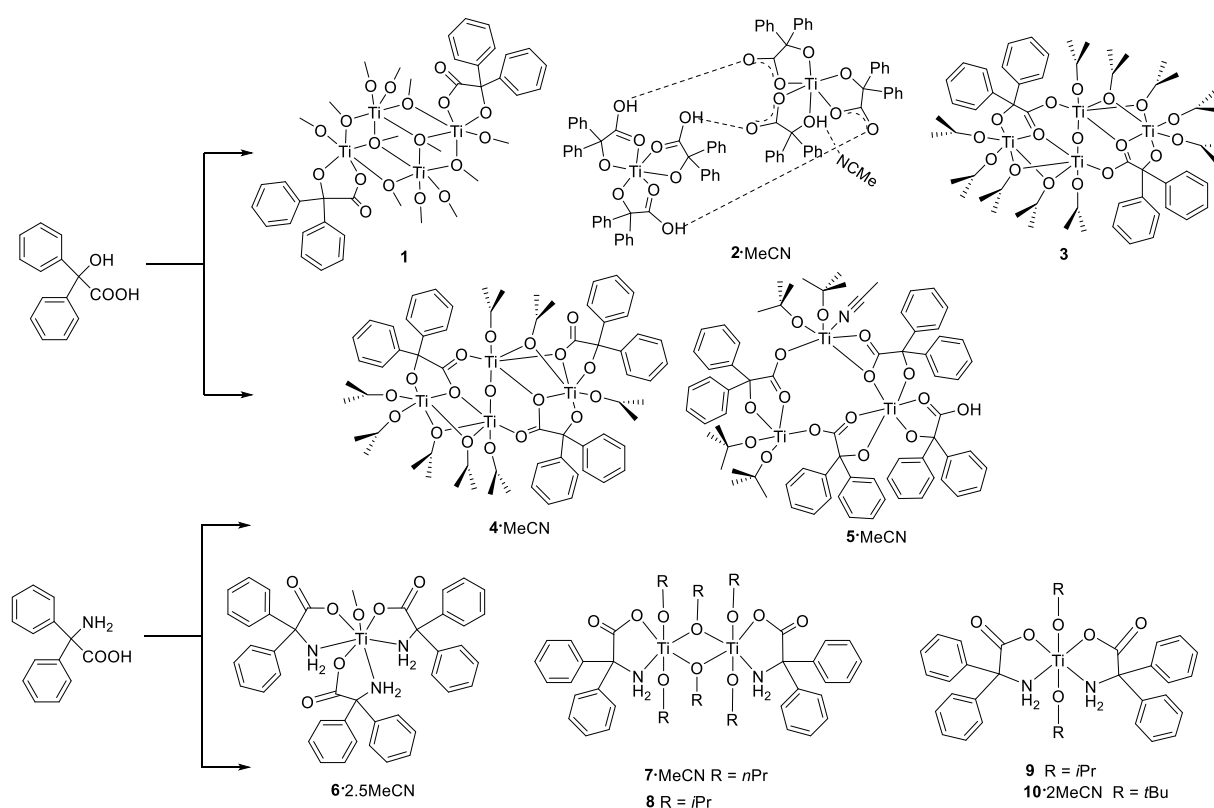


Copyright: © 2022 by the authors. Licensee MDPI, Basel, Switzerland. This article is an open access article distributed under the terms and conditions of the Creative Commons Attribution (CC BY) license (<https://creativecommons.org/licenses/by/4.0/>).

1. Introduction

The current issues associated with plastics and the environment are driving the search for greener alternatives to petroleum-derived products. One option that has attracted attention in recent years as a route to accessing biodegradable polymers is the ring opening polymerization (ROP) of cyclic esters [1–11]. Notable successes include the polymers polycaprolactone (PCL) and polylactide (PLA), and to a lesser extent polyvalerolactone (PVL), which have seen widespread application, for example in the packaging and medical industries [12–14]. As the demand grows for the more extensive use of such materials, it will be important to have access to a wide range of polymers with combinations of desirable properties, such as strength and biodegradability. To achieve this, one available option is to develop new, efficient, metal-based initiators by manipulation of the coordination environment about the metal center. With this in mind, we note that the use of chelating ligands with a variety of metals has proved particularly fruitful [15–18], whilst the use of multi-metallic systems can also be beneficial [19–27]. One issue when using multimetallic systems is their unambiguous characterization, and it is often necessary to determine the molecular structure by single crystal X-ray diffraction. In turn, this requires the use of highly crystalline catalysts, and with this in mind, we note that the $\text{Ph}_2\text{C}(\text{X})$

motif promotes highly crystalline samples, as first recognized by Braun [28,29]. Taking advantage of this, but also noting that the solubility should not be compromised to any great degree, we have been investigating the use of chelate ligands derived from the acids $\text{Ph}_2\text{C}(\text{X})\text{CO}_2\text{H}$, where $\text{X} = \text{OH}$ and NH_2 , and have isolated ROP catalysts based on Li, Al, Zn, rare earth metals [30–33], and more recently Nb and Ta [34]; copper complexes proved to be inactive [35]. However, the coordination chemistry of these acids is rather limited, and transition metal examples are scant [30–42]. Herein, we report our investigations on the use of titanium alkoxides when combined with these acids, and report some intriguing multimetallic structural motifs (Scheme 1). These acid/alkoxide products have afforded ROP catalyst systems exhibiting reasonable activities and low polydispersities (PDIs). We note that the use of multidentate ligation in titanium in catalytic systems for biopolymer synthesis has been reviewed [43], including a report on the use of amino acid-derived ligation [44]. The coordination chemistry of α -hydroxycarboxylic acids has also attracted interest [45].



Scheme 1. Titanium complexes bearing chelate ligands derived from benzilic acid (L^1H_2) (1–5), and 2,2'-diphenylglycine (L^2H_3) (6–10).

2. Results and Discussion

2.1. Synthesis and Characterization of Ti Complexes

2.1.1. Benzilic Acid (L^1H_2)-Derived Complexes

Our initial studies have focused on the use of benzilic acid, given that it is available in bulk quantities and at relatively low costs [46]. The reactions of L^1H_2 with differing ratios (see Scheme 1) of the titanium tetraalkoxides $[\text{Ti}(\text{OR})_4]$ ($\text{R} = \text{Me}$, $n\text{Pr}$, $i\text{Pr}$, $t\text{Bu}$) have been studied, and we report here only the systems where the products obtained were suitable for characterization using single crystal X-ray crystallography. The compounds were also characterized by ^1H NMR and FTIR spectroscopy, mass spectrometry and elemental analysis. All reactions were conducted in refluxing toluene, followed by workup (extraction) using warm acetonitrile, and recrystallization upon standing (2–3 days) at ambient temperature, unless stated otherwise.

Complex **1** was synthesized by using a 1:2 mole ratio of L^1H_2 to $[Ti(OMe)_4]$ affording a highly crystalline product **1** in reasonable isolated yield (*ca.* 50%). The molecular structure of $[Ti_4(L^1)_2(OMe)_{12}]$ (**1**) is shown in Figure 1, with selected bond lengths and angles given in the caption. Complex **1** crystallizes as centrosymmetric clusters composed of four Ti ions in octahedral coordination that are arranged in a diamond shape. These are bridged by a pair of μ_3 -OMe above and below the plane of the four Ti ions. There are four further μ_2 -OMe ligands that form the edges of the diamond. For a *trans* pair of Ti ions, the coordination is completed by two further terminal OMe ligands. For the two other Ti ions, the coordination is completed by one OMe and chelating benzylate²⁻; the benzoic acid plays no part in linking titanium ions. For this structure and others herein, it is possible to classify the coordination mode of the benzylate using the Harris notation [47], and there is further detail in the Supporting Information (Figure S1). Here, the coordination of the benzylate can be classified as [1.011]. The asymmetric unit (Figure 1) contains two independent half clusters. For a further representation of this structure, see the Supporting Information (Figure S2). There are no classical hydrogen bonds present, but there are C–H \cdots O interactions between the clusters.

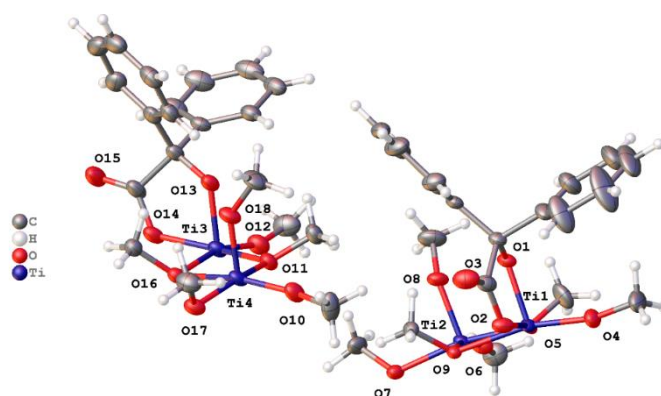


Figure 1. Asymmetric unit of **1** with atoms drawn as 50% probability ellipsoids. (Two symmetry-independent half clusters are present). Selected bond lengths (Å) and bond angles (°): Ti(1)–O(4) 1.7660(17), Ti(1)–O(1) 1.8556(16), Ti(1)–O(5) 1.9750(18), Ti(1)–O(2) 1.9800(18), Ti(1)–O(7#1) 2.0173(16), Ti(1)–O(9) 2.2140(15), Ti(2)–O(6) 1.7446(18), Ti(2)–O(8) 1.8031(16), Ti(2)–O(7) 1.9912(16), Ti(2)–O(5) 2.0125(16), Ti(2)–O(9) 2.1424(16), Ti(2)–O(9#1) 2.1847(15); O(4)–Ti(1)–O(1) 101.14(8), O(4)–Ti(1)–O(5) 99.31(8), O(1)–Ti(1)–O(5) 94.61(7), O(4)–Ti(1)–O(2) 100.41(8), O(1)–Ti(1)–O(2) 79.78(7), O(5)–Ti(1)–O(2) 160.19(7), O(4)–Ti(1)–O(7#1) 93.61(7), O(1)–Ti(1)–O(7#1) 162.32(7), O(5)–Ti(1)–O(7#1) 92.56(7), O(2)–Ti(1)–O(7#1) 88.05(7), O(4)–Ti(1)–O(9) 165.98(7), O(1)–Ti(1)–O(9) 92.08(6), O(5)–Ti(1)–O(9) 74.74(6), O(2)–Ti(1)–O(9) 86.41(7), O(6)–Ti(2)–O(8) 101.52(8), O(6)–Ti(2)–O(7) 97.57(8), O(8)–Ti(2)–O(7) 93.87(7), O(6)–Ti(2)–O(5) 94.09(8), O(8)–Ti(2)–O(5) 96.89(7), O(7)–Ti(2)–O(5) 162.23(7), O(6)–Ti(2)–O(9) 163.42(8), O(8)–Ti(2)–O(9) 92.73(7), O(7)–Ti(2)–O(9) 89.79(7), O(5)–Ti(2)–O(9) 75.64(6), O(6)–Ti(2)–O(9#1) 95.55(7), O(8)–Ti(2)–O(9#1) 160.96(7).

Similar use of $[Ti(OMe)_4]$ with L^1H_2 in a ratio of 1:2 led to the isolation of the salt complex $[Ti(L^1H)_3][Ti(L^1H)(L^1H)_2] \cdot MeCN$ (**2**·MeCN). Complex **2**·MeCN crystallizes in the monoclinic space group $P2_1/c$. The asymmetric unit (Figure 2) contains two independent six-coordinate titanium ions, each of which is coordinated by three bidentate benzylate ions in a *fac* arrangement. For the first titanium ion, Ti1, each benzoic acid is deprotonated only at the alcohol so that it chelates through the alkoxide and the carbonyl of the carboxylic acid, and formally, the coordination of each benzylate is [1.011]. The OH portion of each carboxylic acid forms a hydrogen bond to the neighbouring cluster centered on Ti2. In this way, there are hydrogen-bonded dimers.

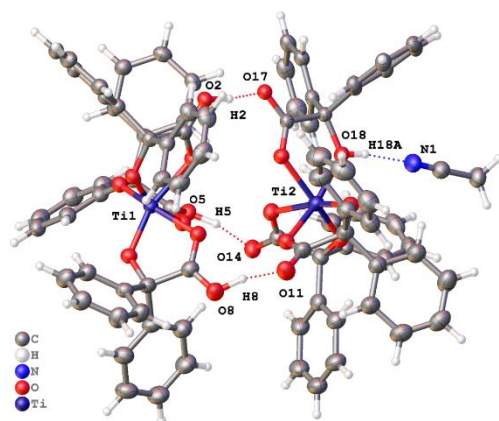


Figure 2. Asymmetric unit of **2** with atoms drawn as 50% probability ellipsoids. Dashed lines show classical hydrogen bonds. Selected bond lengths (Å) and bond angles (°): Ti(1)–O(1) 2.0679(18), Ti(1)–O(3) 1.8377(18), Ti(1)–O(4) 2.0880 (19), Ti(1)–O(6) 1.8550 (19), Ti(1)–O(7) 2.097(2), Ti(1)–O(9) 1.8438(19); O(3)–Ti(1)–O(4) 161.49(8), O(3)–Ti(1)–O(6) 100.04(8), O(3)–Ti(1)–O(7) 96.16(8), O(3)–Ti(1)–O(9) 102.00(8), O(4)–Ti(1)–O(7) 84.34(8), O(6)–Ti(1)–O(1) 95.44(8), O(6)–Ti(1)–O(4) 77.91(8), O(6)–Ti(1)–O(7) 162.15(8), O(9)–Ti(1)–O(1) 158.84(8), O(9)–Ti(1)–O(4) 96.24(8), O(9)–Ti(1)–O(6) 105.17(9), O(9)–Ti(1)–O(7) 78.51(8).

The coordination about Ti2 is similar (See the Supporting Information, Figure S3); two of the three benzoic acids are twice deprotonated, but the third is deprotonated only at the carboxylic acid. All are chelating in [1.011] mode. The alcohol does bind to Ti2, but also forms a hydrogen bond to an unbound molecule of acetonitrile. The X-ray scattering data were good enough that it was possible to identify the positions of the hydrogen atoms through difference Fourier methods.

In the case of $[\text{Ti}(\text{O}i\text{Pr})_4]$, varying the reaction stoichiometry led to the isolation of two different products. When using a ratio of 1:2 ($\text{L}^1\text{H}_2:\text{Ti}$), the product isolated was found to be $[\text{Ti}_4\text{OL}^1_2(\text{O}i\text{Pr})_{10}]$ (**3**). The clusters (Figure 3) in **3** contain four roughly octahedral Ti ions that are linked by benzoate, each of which has a $[3.1_12_{23}1_3]$ coordination mode, and by bridging isopropoxide; for an alternative view, see Supporting Information (Figure S4). The cluster can be described by dividing it into two similar halves. Benzoate is chelated to Ti1, but the carboxylate is also involved in bonding to Ti2 and Ti3. Ti1 and Ti2 are further linked by two μ_2 -*OiPr*, and terminal *OiPr* ligands complete the coordination at Ti1 and Ti2. Ti4 and Ti3 are akin to Ti1 and Ti2, and the two halves are linked by the two Ti–O carboxylate bonds and an oxide bridge. The average Ti···Ti bond distance in the two halves of the cluster is 3.059(4) Å, which is similar to the value of 3.0459(7) Å in the oxo-bridged tetranuclear titanium compound reported by Kemmitt et al. [48], and is indicative of no Ti–Ti bonding.

On changing the ratio to 1:1, the product isolated was $[\text{Ti}_4\text{O}(\text{L}^1)_3(\text{O}i\text{Pr})_8]$ (**4**), which crystallizes in the triclinic system in the space group *P*-1 (Figure 4; an alternative view is given in the Supporting Information, Figure S5). Complex **4** is very similar to **3**, but one terminal *OiPr* ligand and one bridging *OiPr* ligand on Ti1 are replaced by a chelating benzoate, which also bridges to Ti2 in the coordination mode [2.021]. Each of the other two benzoate anions have $[3.1_12_{23}1_3]$ coordination mode, being both chelating and bridging. There is substantial disorder in the position and orientation of the ligand set, particularly around Ti4. There is also evidence of a small amount of disordered solvent equating to one acetonitrile per cluster. The Ti···Ti distances are 3.0682(10), 3.2583(12), and 3.3958(11) Å, which are notably longer than observed in **3**.

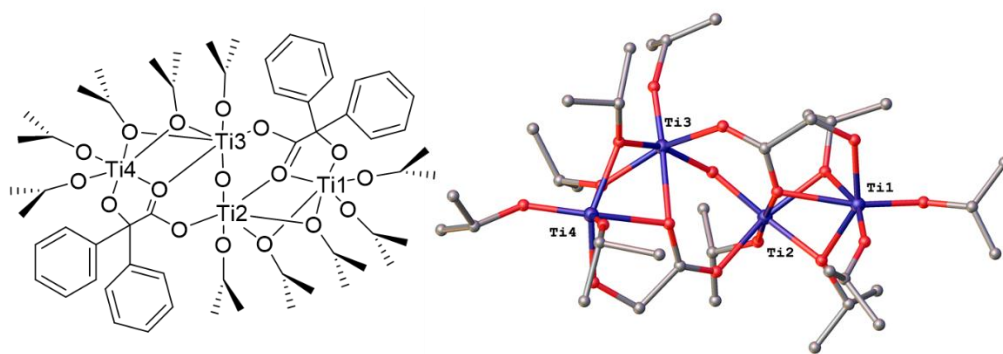


Figure 3. Asymmetric unit of **3**. For clarity, atoms are drawn as spheres of arbitrary radius, minor disorder is not shown, and hydrogen atoms are not shown. Selected bond lengths (Å) and bond angles (°): Ti(1)-O(1) 2.136(8), Ti(1)-O(3) 1.888(9), Ti(1)-O(7) 1.832(9), Ti(1)-O(8) 1.697(10), Ti(1)-O(9) 2.277(9), Ti(1)-O(10) 2.022(8), Ti(2)-O(1) 2.260(7), Ti(2)-O(5) 2.075(8), Ti(2)-O(9) 1.963(9), Ti(2)-O(10) 2.028(8), Ti(2)-O(11) 1.799(7), Ti(2)-O(17) 1.766(8); O(1)-Ti(1)-O(9) 72.1(3), O(3)-Ti(1)-O(1) 76.0(3), O(3)-Ti(1)-O(10) 149.1(3), O(7)-Ti(1)-O(1) 163.5(3), O(7)-Ti(1)-O(10) 106.3(4), O(8)-Ti(1)-O(1) 94.9(4), O(8)-Ti(1)-O(3) 99.6(4), O(8)-Ti(1)-O(7) 101.5(4), O(8)-Ti(1)-O(9) 160.2(4), O(8)-Ti(1)-O(10) 92.1(4), O(10)-Ti(1)-O(1) 74.6(3), O(10)-Ti(1)-O(9) 70.4(3), O(5)-Ti(2)-O(1) 84.7(3), O(9)-Ti(2)-O(1) 75.6(3), O(9)-Ti(2)-O(5) 156.4(3), O(9)-Ti(2)-O(10) 77.1(3), O(10)-Ti(2)-O(1) 71.8(3), O(10)-Ti(2)-O(5) 84.5(3), O(11)-Ti(2)-O(9) 102.6(3), O(11)-Ti(2)-O(10) 155.6(3), O(17)-Ti(2)-O(1) 175.3(3), O(17)-Ti(2)-O(5) 92.9(3), O(17)-Ti(2)-O(9) 105.8(4), O(17)-Ti(2)-O(10) 104.0(3), O(17)-Ti(2)-O(11) 99.5(3).

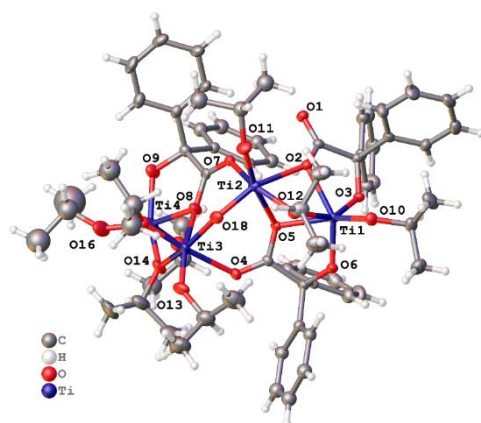


Figure 4. Asymmetric unit of **4** with atoms drawn as 50% probability ellipsoids. Disorder is not illustrated. Selected bond lengths (Å) and bond angles (°): Ti(1)-O(5) 2.204(3), Ti(1)-O(3) 1.829(3), Ti(1)-O(2) 2.096(3), Ti(1)-O(6) 1.860(3), Ti(1)-O(10) 1.787(3), Ti(1)-O(12) 2.059(3), Ti(2)-O(5) 2.159(3), Ti(2)-O(7) 2.055(3), Ti(2)-O(2) 2.160(3), Ti(2)-O(12) 1.968(3), Ti(2)-O(18) 1.762(3), Ti(2)-O(11) 1.765(3), Ti(3)-O(4) 2.188(3), Ti(3)-O(18) 1.856(4), Ti(3)-O(8) 2.208(3), Ti(3)-O(14) 2.020(4), Ti(3)-O(13) 1.765(3), Ti(3)-O(17) 1.840(5), Ti(3)-O(17A) 1.907(9), Ti(4)-O(8) 2.098(3), Ti(4)-O(9) 1.884(4), Ti(4)-O(14) 1.957(4), Ti(4)-O(16) 1.757(4), Ti(4)-O(15) 1.830(5), Ti(4)-O(15A) 1.643(10), Ti(4)-O(17A) 2.458(9); O(3)-Ti(1)-O(5) 102.26(11), O(3)-Ti(1)-O(2) 77.55(11), O(3)-Ti(1)-O(6) 99.49(12), O(3)-Ti(1)-O(12) 150.55(12), O(2)-Ti(1)-O(5) 70.52(10), O(6)-Ti(1)-O(5) 75.37(11), O(6)-Ti(1)-O(2) 144.11(12), O(6)-Ti(1)-O(12) 106.64(12), O(10)-Ti(1)-O(5) 159.81(12), O(10)-Ti(1)-O(3) 97.89(13), O(10)-Ti(1)-O(2) 115.59(13), O(10)-Ti(1)-O(6) 100.28(13), O(10)-Ti(1)-O(12) 90.68(13), O(5)-Ti(2)-O(2) 70.24(10), O(7)-Ti(2)-O(5) 84.82(11), O(7)-Ti(2)-O(2) 85.14(10), O(12)-Ti(2)-O(5) 74.96(11), O(12)-Ti(2)-O(7) 154.61(11), O(12)-Ti(2)-O(2) 73.77(11), O(18)-Ti(2)-O(5) 87.37(12), O(18)-Ti(2)-O(7) 93.96(14), O(18)-Ti(2)-O(2) 157.59(13), O(18)-Ti(2)-O(12) 100.18(14), O(18)-Ti(2)-O(11) 103.86(15), O(11)-Ti(2)-O(5) 168.77(13), O(11)-Ti(2)-O(7) 94.08(14), O(11)-Ti(2)-O(2) 98.54(13), O(9)-Ti(4)-O(8) 75.54(13), O(9)-Ti(4)-O(14) 143.93(16), O(14)-Ti(4)-O(8) 73.34(13).

Finally, we investigated the use of $[\text{Ti}(\text{O}t\text{Bu})_4]$, and found that the use of a 1:1 ratio resulted in the formation of the asymmetric trinuclear titanium complex $[\text{Ti}_3(\text{L}^1)_4(\text{O}t\text{Bu})_4 \cdot \text{MeCN}] \cdot \text{MeCN}$

(5-MeCN) (Figure 5; an alternative view is given in the Supporting Information, Figure S6). Complex 5 crystallizes in the triclinic system with the space group $P-1$. This features a cluster composed of Ti ions bridged by benzilate and decorated by two monodentate *Ot*Bu ligands as each of Ti2 and Ti3. At Ti1, there is chelating, but not bridging benzilate. Here, there are four unique benzilate anions, and these feature three different coordination modes. At Ti1, the alkoxide and carboxylic acid form a five-membered chelate (benzilate coordination mode [2.011]); one further ion forms a similar chelate, but the second oxygen of the carboxylate bonds to Ti2 (coordination mode [2.1₁1₂1₂]); the third chelating anion forms a similar five-membered chelate, but in addition to this the carboxylate forms an unequal bidentate chelate to Ti3, such that one of the oxygen atoms (O4) bridges between Ti1 and Ti3 in coordination mode [2.1₁2₁₂1₂]. The M–O bond lengths for the bidentate chelating carboxylate are these: Ti3–O4 2.3458(8) Å and Ti3–O5 2.0624(8) Å. Ti2 and Ti3 are joined by a “normal” chelating anion that also bridges through the second oxygen of the carboxylate (coordination mode [2.1₁1₂1₂]).

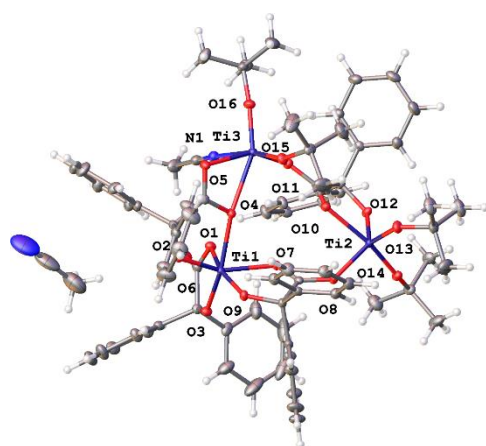


Figure 5. Asymmetric unit of 5 with atoms drawn as 50% probability ellipsoids. Selected bond lengths (Å) and bond angles (°): Ti(1)–O(10) 1.7393(10), Ti(1)–O(9) 1.7389(10), Ti(1)–O(6) 1.9703(10), Ti(1)–O(1) 2.0623(10), Ti(1)–N(5) 2.2675(13), Ti(1)–O(2) 2.3456(10), Ti(2)–O(16) 1.8371(10), Ti(2)–O(14) 1.8548(10), Ti(2)–O(15) 1.8580(10), Ti(2)–O(3) 2.0173(10), Ti(2)–O(7) 2.0834(10), Ti(2)–O(2) 2.1848(10), Ti(3)–O(12) 1.7699(10), Ti(3)–O(11) 1.7773(10), Ti(3)–O(13) 1.8650(10), Ti(3)–O(8) 1.9827(10), Ti(3)–O(5) 2.1213(10); O(10)–Ti(1)–O(9) 104.31(5), O(14)–Ti(2)–O(15) 97.49(4), O(11)–Ti(3)–O(8) 108.43(5), O(10)–Ti(1)–O(6) 97.48(4), O(16)–Ti(2)–O(3) 80.13(4), O(13)–Ti(3)–O(8) 131.22(4), O(9)–Ti(1)–O(6) 101.45(4), O(14)–Ti(2)–O(3) 162.34(4), O(12)–Ti(3)–O(5) 161.99(4), O(10)–Ti(1)–O(1) 95.97(4), O(15)–Ti(2)–O(3) 100.09(4), O(11)–Ti(3)–O(5) 92.60(4), O(9)–Ti(1)–O(1) 102.02(4), O(6)–Ti(1)–O(1) 149.05(4), O(8)–Ti(3)–O(5) 80.33(4), O(10)–Ti(1)–N(5) 167.84(5), O(15)–Ti(2)–O(7) 154.51(4), O(9)–Ti(1)–N(5) 87.85(5), O(3)–Ti(2)–O(7) 85.27(4), O(16)–Ti(2)–O(2) 161.52(4), O(1)–Ti(1)–N(5) 81.25(4), O(14)–Ti(2)–O(2) 100.77(4), O(10)–Ti(1)–O(2) 92.13(4), O(15)–Ti(2)–O(2) 77.03(4), O(9)–Ti(1)–O(2) 156.56(4), O(3)–Ti(2)–O(2) 81.60(4), O(6)–Ti(1)–O(2) 92.67(4), O(7)–Ti(2)–O(2) 79.18(4), O(1)–Ti(1)–O(2) 59.04(4), O(12)–Ti(3)–O(11) 105.13(5), N(5)–Ti(1)–O(2) 76.26(4), O(16)–Ti(2)–O(14) 97.48(4), O(11)–Ti(3)–O(13) 115.14(5), O(16)–Ti(2)–O(15) 103.48(4), O(12)–Ti(3)–O(8) 96.65(4), O(11)–Ti(3)–O(8) 108.43(5), O(13)–Ti(3)–O(8) 131.22(4), O(12)–Ti(3)–O(5) 161.99(4), O(11)–Ti(3)–O(5) 92.60(4), O(8)–Ti(3)–O(5) 80.33(4).

2.1.2. Infrared and ¹H NMR Spectra of Benzilic-Derived Complexes

In the FT-IR spectra, for the parent L^1H_2 , there is a sharp and intense peak at 3395 cm^{-1} , corresponding to the ν O–H asymmetric stretching vibration. However, this O–H peak for complexes 1–5 has disappeared, which verifies the participation of the hydroxyl group in the reaction. The ν C = O stretching vibration in L^1H_2 gives rise to a sharp band at 1716 cm^{-1} , whereas the C = O stretching shifts to 1680 cm^{-1} , 1733 cm^{-1} , 1729 cm^{-1} , 1728 cm^{-1} and 1704 cm^{-1} for 1–5, respectively, indicative of bonding between the carboxyl and the titanium center. A new band appeared for all the complexes in the range $429\text{--}466\text{ cm}^{-1}$, which we assign to Ti–O bonding. The ¹H NMR spectra suggest alkoxide exchange takes place in

the solution for the L^1H_2 -derived complexes containing bridging and terminal alkoxide ligation. However, VT 1H NMR spectroscopic studies (in CD_3CN) conducted between -40 °C and $+50$ °C revealed little change; overall integrations were consistent with the solid-state structures, e.g., the integral ratio of the multi-signals for the phenyl groups ($\delta = 7.83$ – 6.80), the septet for the isopropoxide methine ($\delta = 3.89$ – 3.83 and 3.32) and the doublet for the methyls ($\delta = 1.07$ and 1.06) are 20:10:60 consistent with the structure of **3**. The structures of the complexes are also consistent with their elemental analysis and mass spectrometry data.

2.1.3. Diphenylglycine (L^2H_3)-Derived Complexes

Having established suitable synthetic conditions for the synthesis and isolation of titanium complexes derived from L^1H_2 , we extended our studies to the somewhat more expensive 2,2'-diphenylglycine, $Ph_2C(NH_2)CO_2H$ (L^2H_3) [49]. In every complex, this ligand is deprotonated by the acid and displays a simple five-membered chelate with Harris notation [1.011]. In the case of $[Ti(OMe)_4]$, the use of a 2:1 ratio (L^2H_3 :Ti) resulted in the isolation of the complex $[Ti(L^2)_3OMe] \cdot 2.5MeCN$ (**6**· $2.5MeCN$), which crystallizes in the monoclinic space group $I2/a$. The asymmetric unit comprises a discrete seven-coordinate Ti complex (Figure 6), where the Ti is surrounded by three chelating diphenylglycinate ligands and one OMe ligand. Two chelating ligands and the NH_2 from another lie approximately in a plane with the carboxylate filling an axial position; the other axial position is filled by methoxide. The ligands are arranged such that two N–H bonds from different bound amines form hydrogen bonds to a carbonyl in an adjacent complex. These interactions generate a hydrogen-bonded chain that runs parallel to the crystallographic b -axis. Subsidiary C–H $\cdots\pi$ interactions form along the direction of these chains and between them (See the Supporting Information, Figure S7).

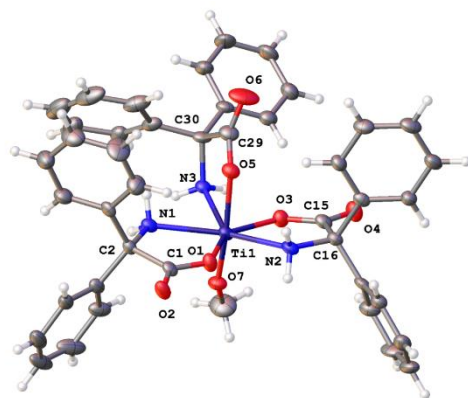


Figure 6. Asymmetric unit of **6**· $2.5MeCN$ with atoms drawn as 50% probability ellipsoids. Selected bond lengths (Å) and bond angles (°): Ti(1)–O(5) 1.984(2), Ti(1)–O(1) 2.019(2), Ti(1)–O(7) 1.772(2), Ti(1)–O(3) 2.042(2), Ti(1)–N(3) 2.245(3), Ti(1)–N(1) 2.262(3), Ti(1)–N(2) 2.237(3); O(5)–Ti(1)–O(1) 93.65(9), O(5)–Ti(1)–O(3) 88.84(10), O(5)–Ti(1)–N(3) 75.90(9), O(5)–Ti(1)–N(1) 85.75(10), O(5)–Ti(1)–N(2) 85.17(10), O(1)–Ti(1)–O(3) 141.47(9), O(1)–Ti(1)–N(3) 146.56(10), O(1)–Ti(1)–N(1) 72.62(9), O(1)–Ti(1)–N(2) 70.49(9), O(7)–Ti(1)–O(5) 168.79(10), O(7)–Ti(1)–O(1) 95.69(10), O(7)–Ti(1)–O(3) 87.71(10), O(7)–Ti(1)–N(3) 92.89(10), O(7)–Ti(1)–N(1) 91.13(11), O(7)–Ti(1)–N(2) 103.79(11), O(3)–Ti(1)–N(3) 71.00(10), O(3)–Ti(1)–N(1) 145.83(9), O(3)–Ti(1)–N(2) 71.43(9), N(3)–Ti(1)–N(1) 74.96(10), N(2)–Ti(1)–N(3) 137.96(10), N(2)–Ti(1)–N(1) 141.26(10).

The use of $[Ti(OnPr)_4]$ in a 1:1 ratio afforded, following work-up, yellow crystals of $[Ti_2(L^2)_2(OnPr)_6]$ (**7**). The structure contains a distorted octahedral coordination of titanium; each Ti has two $OnPr$ ligands that bridge to another equivalent Ti to form centrosymmetric dimers. Each Ti bears on chelating diphenylglycinate, two monodentate alkoxides and two bridging alkoxides. The asymmetric unit contains two symmetrically unique halves of the dimer, as shown below (Figure 7).

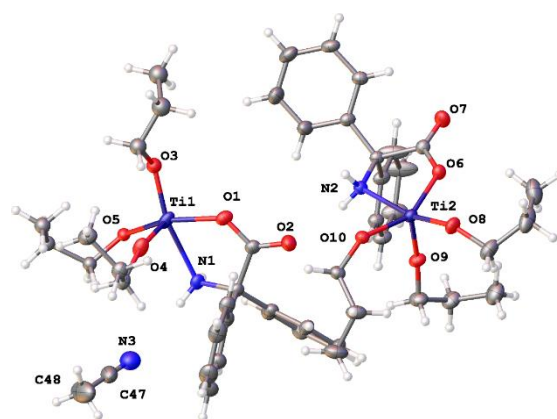


Figure 7. Asymmetric unit of 7 with atoms drawn as 50% probability ellipsoids. For clarity, minor disorder is not shown. Selected bond lengths (Å) and bond angles (°): Ti(1)-Ti(1i) 3.2815(5), Ti(1)-O(1) 1.9868(13), Ti(1)-O(3) 1.8486(17), Ti(1)-O(4) 1.7717(12), Ti(1)-O(5) 2.048 (3), Ti(1)-N(1) 2.2829(14); O(5)-Ti(1)-O(1) 152.78(8), O(5)-Ti(1)-O(4) 96.15(9), O(5)-Ti(1)-N(1) 84.55(8), O(5)-Ti(1)-O(3) 104.04(9), O(4)-Ti(1)-O(1) 100.20(5), O(4)-Ti(1)-O(3) 100.42(7), O(4)-Ti(1)-N(1) 88.62(6), O(3)-Ti(1)-O(1) 94.27(6), O(3)-Ti(1)-N(1) 166.64(7), O(1)-Ti(1)-N(1) 74.31(5), Ti(1)-O(5A)-Ti(1i) 114.10 (18).

The action of the inversion center generates a dimer from two Ti1 centres and a dimer from two Ti2 centers. There are intramolecular N–H···O (alkoxide) hydrogen bonds that help to stabilize the dimers and N–H···O(carbonyl) hydrogen bonds between adjacent complexes that form 1-D chains that run parallel to the crystallographic [1,1,1] direction. Views of the coordination about Ti1 and Ti2 are shown in the Supporting Information (Figure S8).

The similar use of $[\text{Ti}(\text{O}i\text{Pr})_4]$ also resulted in the formation of a dinuclear complex, namely, $[\text{Ti}_2(\text{L}^2)_2(\text{O}i\text{Pr})_6]$ (8). Although the crystal structure is somewhat different (Figure 8; for an alternative view, see the Supporting Information, Figure S9), the basic cluster present in 8 is essentially the same as in 7; two Ti ions are bridged by a pair of alkoxides, and the coordination about each Ti ion is completed by terminal alkoxide ligands and bidentate diphenylglycinate. Intramolecular hydrogen bonding between NH_2 and alkoxide is also present, but there are no classical hydrogen bonds between the clusters, which is the major difference between 7 and 8. The carbonyl of the carboxylic acid forms C–H···O intermolecular interactions with two different complexes. These interactions extend in 3D throughout the crystal structure.

Upon changing the ratio to 2:1 ($\text{L}^2\text{H}_3:\text{Ti}$), the use of $[\text{Ti}(\text{O}i\text{Pr})_4]$ led to the isolation of the mononuclear complex $[(\text{L}^2\text{H}_2)_2\text{Ti}(\text{O}i\text{Pr})_2]$ (9), the molecular structure of which is shown in Figure 9 (an alternative view is given in the Supporting Information, Figure S10). This features a rather distorted octahedral coordination about the Ti composed of two *cis* diphenylglycinate ligands and two terminal isopropoxide ligands, such that there is close to a local twofold axis at the metal center between the two Ti–N bonds. The two nitrogen donor atoms are adjacent, but the two oxygen atoms of the chelates are trans at the metal. The asymmetric unit has three symmetrically unique complexes that have the same coordination but differ very slightly in the orientation of the methyl groups of the isopropoxide. The three unique complexes are aligned along the crystallographic *a*-axis to form an infinite rank of these complexes in the crystal structure. Between each and every pair of adjacent complexes, there is a pseudo-centrosymmetric pair of N–H···O hydrogen bonds. There is evidence of C–H···O and C–H··· π interactions between these ranks.

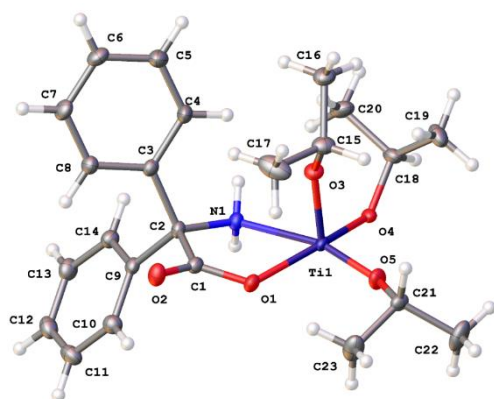


Figure 8. Asymmetric unit of **8** with atoms drawn as 50% probability ellipsoids. For clarity, minor disorder is not shown. Selected bond lengths (Å) and bond angles (°): Ti(1)-Ti(1ⁱ) 3.2788(4), Ti(1)-O(4) 1.9618(9), Ti(1)-O(4ⁱ) 2.1357(9), Ti(1)-O(1) 1.9945(10), Ti(1)-O(3) 1.7990(9), Ti(1)-O(5) 1.7884(9), Ti(1)-N(1) 2.2901(10), Ti(1)-Ti(1ⁱ) 3.2788(4); O(4)-Ti(1)-O(4ⁱ) 73.78(4), O(4)-Ti(1)-O(1) 155.56(4), O(4ⁱ)-Ti(1)-N(1) 81.69(4), O(4)-Ti(1)-N(1) 87.18(4), O(1)-Ti(1)-O(4ⁱ) 89.31(4), O(1)-Ti(1)-N(1) 72.73(4), O(3)-Ti(1)-O(4ⁱ) 167.74(4), O(3)-Ti(1)-O(4) 98.25(4), O(3)-Ti(1)-O(1) 95.14(4), O(3)-Ti(1)-N(1) 88.71(4), O(5)-Ti(1)-O(4ⁱ) 91.32(4), O(5)-Ti(1)-O(4) 104.07(4), O(5)-Ti(1)-O(1) 93.62(4), O(5)-Ti(1)-O(3) 99.77(5), O(5)-Ti(1)-N(1) 164.63(4), Ti(1)-O(4)-Ti(1ⁱ) 106.22(4).

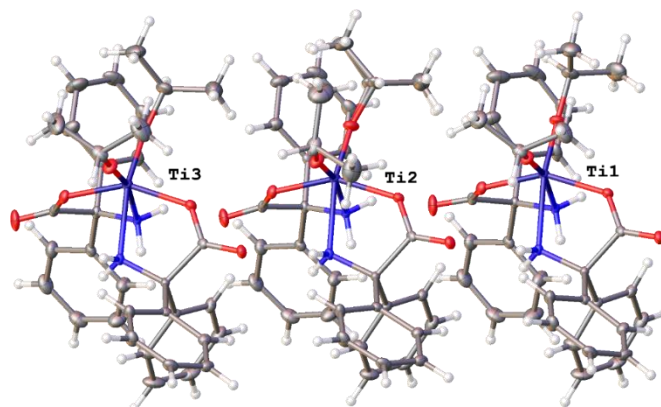


Figure 9. Asymmetric unit of **9** with atoms drawn as 50% probability ellipsoids. For clarity, some minor disorder is not shown. Selected bond lengths (Å) and bond angles (°): Ti(1)-O(3) 1.7658(14), Ti(1)-O(4) 1.7686(14), Ti(1)-O(2) 1.9786(14), Ti(1)-O(5) 1.9847(14), Ti(1)-N(2) 2.2508(16), Ti(1)-N(1) 2.3025(16); O(3)-Ti(1)-O(4) 103.37(7), O(3)-Ti(1)-O(2) 96.33(6), O(4)-Ti(1)-O(2) 98.45(6), O(3)-Ti(1)-O(5) 97.81(6), O(4)-Ti(1)-O(5) 102.24(6), O(2)-Ti(1)-O(5) 151.42(6), O(3)-Ti(1)-N(2) 167.16(7), O(4)-Ti(1)-N(2) 88.06(6), O(2)-Ti(1)-N(2) 87.59(6), O(5)-Ti(1)-N(2) 73.72(5), O(3)-Ti(1)-N(1) 86.36(6), O(4)-Ti(1)-N(1) 168.37(6), O(2)-Ti(1)-N(1) 73.83(6), O(5)-Ti(1)-N(1) 82.42(6), N(2)-Ti(1)-N(1) 83.00(6).

Interestingly, interaction of L^2H_3 with $[Ti(OtBu)_4]$ using a ratio of 1:1 resulted in the formation of a similar mononuclear complex $[(L^2H_2)Ti(OtBu)_2] \cdot 2MeCN$ (**10**·2MeCN) (as shown in Figure 10). The basic complex here is very similar to that in **9**, but the intermolecular interactions present are different, which perhaps reflects the inclusion of solvent in the crystal structure. Each discrete complex contains a pair of chelating diphenylglycinate ligands and two terminal *OtBu* ligands, but there is no local twofold axis. The nitrogen donor atoms are adjacent at the metal center, but in contrast to **9**, so are the two oxygen atoms of the chelating ligand. This close approach of the two NH_2 groups means that each of them forms a hydrogen bond to the carboxylate of an adjacent complex, and this forms hydrogen-bonded chains of complexes parallel to the crystallographic *b* direction (see the Supporting Information, Figure S11).

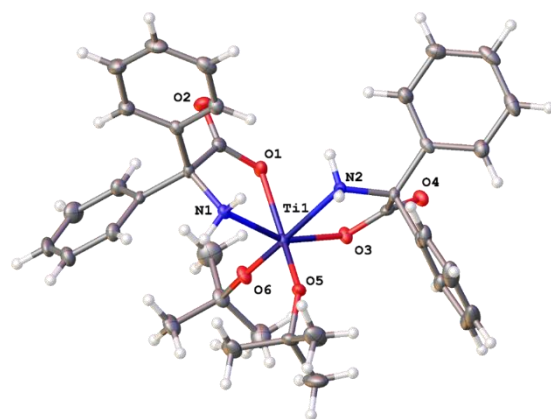


Figure 10. Asymmetric unit of **10**·2MeCN with atoms drawn as 50% probability ellipsoids. For clarity, solvent molecules are not shown. Selected bond lengths (Å) and bond angles (°): Ti(1)–O(6) 1.755(2), Ti(1)–O(5) 1.7747(18), Ti(1)–O(3) 1.9920(18), Ti(1)–O(1) 2.0497(19), Ti(1)–N(1) 2.202(2), Ti(1)–N(2) 2.260(2); O(6)–Ti(1)–O(5) 101.20(9), O(6)–Ti(1)–O(3) 96.38(8), O(5)–Ti(1)–O(3) 105.03(8), O(6)–Ti(1)–O(1) 93.82(9), O(5)–Ti(1)–O(1) 158.53(8), O(3)–Ti(1)–O(1) 88.26(8), O(6)–Ti(1)–N(1) 100.49(9), O(5)–Ti(1)–N(1) 88.48(8), O(3)–Ti(1)–N(1) 155.91(9), O(1)–Ti(1)–N(1) 73.64(7), O(6)–Ti(1)–N(2) 169.12(8), O(5)–Ti(1)–N(2) 87.39(9), O(3)–Ti(1)–N(2) 74.76(8), O(1)–Ti(1)–N(2) 79.81(8), N(1)–Ti(1)–N(2) 86.28(8).

2.1.4. Infrared and ^1H NMR Spectra of the L^2H_3 -Derived Complexes

The infrared spectrum of the parent L^2H_3 contains $\nu\text{N-H}$ stretches at 3269 (sharp), 3180, and 3052 cm^{-1} . A shift ($\sim 90\text{ cm}^{-1}$) of the $\nu\text{N-H}$ was observed for all the diphenylglycine-derived complexes upon coordination with titanium. For example, the IR spectrum of **6**·2.5MeCN contains $\nu\text{N-H}$ at 3335, 3245 and 3055 cm^{-1} , which indicates amine-type bonding is retained in the titanium complexes. Several new peaks appeared for all the complexes in the range of $413\text{--}465\text{ cm}^{-1}$, which is due to the formation of new Ti–O and Ti–N bonds. The solid-state structures of the DpgH-derived complexes are consistent with their ^1H NMR spectra, elemental analysis and mass spectrometry data.

2.2. Ring Opening Polymerization Studies of ϵ -Caprolactone ($\epsilon\text{-CL}$)

Initially, all the complexes were screened for their ability to act as catalysts for the ROP of $\epsilon\text{-CL}$ with a monomer to Ti ratio of 250:1 at $100\text{ }^\circ\text{C}$ under N_2 (Table 1, entries 1 to 10). The complexes **2**, **4** and **5**, which all bear L^1H_2 -derived ligand sets, were found to be the most sluggish even after 24 h, allowing for monomer conversions of 20, 31 and 53%, respectively. The poor activity of **2** was tentatively attributed to the absence of OR groups (other than those derived from L^1), as well as to the two acidic protons reducing the complex's solubility in the reaction medium. Solubility issues could also explain the rather low conversions achieved with **4** and **5**. By contrast, complexes **1** and **3** allowed for complete monomer conversion within 195 min and 150 min, respectively. The isopropoxide-containing complex **3** performed slightly better than the methoxide-bearing **1**. Most catalysts afforded polymers with M_n smaller than the calculated values, except complexes **3** and **10**, albeit with broad polydispersity, allegedly deriving from intramolecular transesterification processes. All complexes bearing L^2H_2 -derived ligands (**6**–**10**) allowed for conversions $\geq 95\%$ within 480 min. An in-situ kinetic study was carried out (using a Youngs tap NMR tube in toluene-d_8) at $100\text{ }^\circ\text{C}$ using a monomer to Ti ratio of 250:1. Figure 11 shows that the ROP using **1**, **3** and **6**–**10** proceed rapidly to full conversion, but over differing time periods. For the L^2H_3 -derived complexes, the *n*-propoxide complex **7** performed best, and its k_{obs} is equal to $4743 \times 10^{-4}/\text{min}$ (Table 2, entry 7). The linearity indicates that the polymerization was first-order in the monomer with rapid initiation and without induction time, but only at $50\text{ }^\circ\text{C}$ (Table 1, run 11) did the behavior approach a living-type character. According to the kinetics of **1**, **3**, **6** and **8**–**10**, the plot of $\ln(\text{CL}_0/\text{CL}_t)$ versus time shows an upward curvature, which implies that polymerization rates increased along with reaction time (Figure 11, left). This type of acceleration phenomenon for ROP

of ϵ -CL has been reported by Basko [50]. If the basicity of the monomer is significantly higher than the polymer unit, the ratio between the activated monomer concentration and the monomer concentration increases as the monomer is consumed, resulting in an apparent speed up of the polymerization. A similar acceleration of kinetics has also been reported by Delcroix [51]. Herein, this was observed for complexes **1**, **3**, **6** and **8–10**, and we calculated k_{obs} after the induction period in order to compare the activities of the different complexes. By contrast, for complexes **2** and **4–5**, there was an obvious induction period; the results are listed in Table 2. For the L^2H_3 -derived complexes **6–10**, k_{obs} follows the sequence $7 \cdot MeCN > 8 > 9 > 10 \cdot 2MeCN > 6 \cdot 2.5MeCN$. Cooperative effects between the two Ti centers of complexes **7** and **8** could explain their superior activity over their monometallic congeners **6**, **9** and **10**. By looking at **7** (*OnPr*) versus **8** (*OiPr*) with near identical structures, *OnPr* has a remarkably positive effect on polymerization, and also facilitates the better control of polymerization (\bar{D} 1.49 versus 1.80); for **9** and **10**, the performance of the *OiPr* exceeds that of the *OiBu*. These differences can be explained in terms of steric hindrance of the alkoxide groups. The lower value of k_{obs} for complex **6** is thought to be due to its poor solubility in toluene/ ϵ -Cl. It is noticeable that for **6**, the reaction mixture remains cloudy at 100 °C, and this likely explains the longest observed induction period. Given the better performance of system **7**, it was selected for further screening. Remarkably, the complex proved able to completely convert up to 2000 equiv. of monomer within minutes at 100 °C (entries 7, 12–14, Table 1). In all cases, the polymers exhibited broad dispersities (up to 2.35), and their M_n values were lower than the calculated values, suggesting the occurrence of undesired intramolecular transesterification reactions. Upon varying the temperature, using a CL:Ti ratio of 250:1, a high conversion was still achieved at 50 °C over 150 min., whilst at ambient temperature (25 °C), the conversion was only 14% after 24 h (Table 1, runs 11 and 15, respectively). By conducting the ROP in the absence of the solvent, complex **7** allowed for $\geq 99\%$ monomer conversion within 6 min., affording a product with a molecular weight of 10.5 kDa (Table 1, run 17). Finally, the catalyst was virtually inactive when carrying out the reaction in air. To better understand the effect of the presence of the chelate, the ROP behavior of the titanium alkoxide starting materials $[Ti(OR)_4]$ ($R = Me, nPr, iPr, tBu$), i.e., ROP in the absence of L^1H_2 - and L^2H_3 -derived ligation, was investigated. The results are presented in Table 1 entries 18–21, which reveal that $[Ti(OnPr)_4]$ allowed for 92% conversion within 2 min, albeit with far less control compared to **1–10** (i.e., broader \bar{D}). We note that the complexes $[Ti(OR)_4]$ can adopt varied structures; for example, tetranuclear has been reported for $R = Me$ (X-ray diffraction [52]) whilst trimeric was observed for $R = nPr$ (cryoscopic measurements) [53]. Complex $[Ti(OnPr)_4]$ is still active for the ROP of ϵ -CL at 100 °C in air; however, the M_w distribution is very broad.

Table 1. ROP of ϵ -CL catalyzed by the Ti complexes **1–10** and $[Ti(OR)_4]$.

Run	Catalyst	L^1/L^2	OR Group	CL:Ti	T (°C)	Time (min)	Conv. ^a (%)	M_n (calc.) ^b (kDa)	M_n (obs.) ^{c,d} (kDa)	\bar{D} ^c
1	1		OMe	250:1	100	195	99	28.3	7.2	1.87
2	2 ·MeCN		-	250:1	100	1440	20	5.7	4.6	1.25
3	3	L^1	<i>OiPr</i>	250:1	100	150	99	28.3	30.0	1.93
4	4 ·MeCN		<i>OiPr</i>	250:1	100	1440	31	8.9	6.0	1.53
5	5 ·MeCN		<i>OiBu</i>	250:1	100	1440	53	15.2	4.1	1.25

Table 1. Cont.

Run	Catalyst	L ¹ /L ²	OR Group	CL:Ti	T (°C)	Time (min)	Conv. ^a (%)	M _n (calc.) ^b (kDa)	M _n (obs.) ^{c,d} (kDa)	D ^c
6	6·2.5MeCN	L ²	OMe	250:1	100	480	95	27.1	6.0	1.22
7	7·MeCN		OnPr	250:1	100	12	99	28.3	8.4	1.49
8	8		OiPr	250:1	100	210	99	28.3	6.7	1.80
9	9		OiPr	250:1	100	345	99	28.3	12.0	1.97
10	10·2MeCN		OtBu	250:1	100	255	99	28.3	39.0	2.41
11	7·MeCN		OnPr	250:1	50	150	99	28.3	4.8	1.20
12	7·MeCN		OnPr	500:1	100	6	99	56.6	13.0	2.35
13	7·MeCN		OnPr	1000:1	100	9	99	113	8.7	1.45
14	7·MeCN		OnPr	2000:1	100	12	99	226	8.6	1.84
15	7·MeCN		OnPr	250:1	25	1440	14	-	-	-
16 ^e	7·MeCN	OnPr	250:1	100	1440	6	-	-	-	
17 ^f	7·MeCN	OnPr	250:1	100	6	98	28.0	10.5	1.29	
18	[Ti(OR) ₄]	-	OMe	250:1	100	195	3	0.9	1.0	1.22
19			OnPr	250:1	100	2	92	26.3	6.7	2.79
20			OiPr	250:1	100	195	94	26.8	7.8	3.01
21			OtBu	250:1	100	195	43	12.3	5.4	2.94
22 ^e			OnPr	250:1	100	2	96	27.4	5.6	3.21

Reaction conditions: ε-CL 4.5 mmol, toluene 2 mL, N₂ atmosphere. ^a Determined by ¹H NMR spectroscopy on the crude reaction mixture. ^b Calculated from [CL]/[Ti] × Conv. × M(CL) + M(end group). ^c From GPC. ^d Values corrected considering Mark–Houwink factor (0.56) from polystyrene standards in THF. ^e Reaction conducted in air. ^f Conducted under solvent-free conditions.

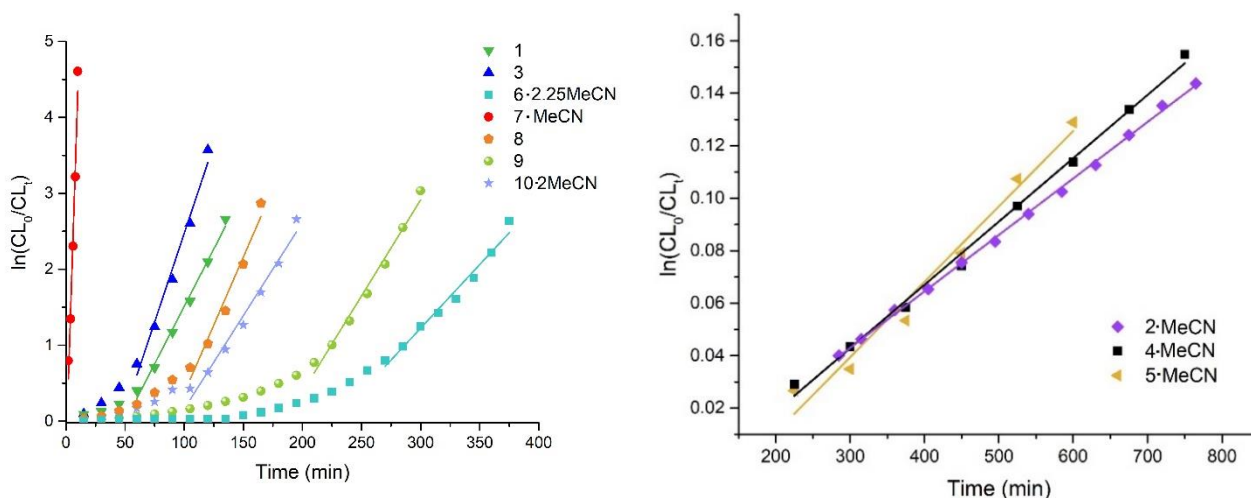


Figure 11. Plot of $\ln(\text{CL}_0/\text{CL}_t)$ versus time. Left: complexes 1, 3 and 6–10; Right: complexes 2, 4 and 5 (Table 1, entries 1–10).

Table 2. Kinetics constants for the ROP of ε-CL catalyzed by 1–10 at 100 °C.

Run	Complex	k_{obs} ($\times 10^4$)	Induction Period (min)
1	1	302 ($R^2 = 0.992$)	60
2	2·MeCN	2.15 ($R^2 = 0.999$)	275
3	3	416 ($R^2 = 0.969$)	60
4	4·MeCN	2.57 ($R^2 = 0.994$)	215
5	5·MeCN	2.87 ($R^2 = 0.977$)	300
6	6·2.5MeCN	159 ($R^2 = 0.977$)	270
7	7·MeCN	4743 ($R^2 = 0.978$)	0
8	8	358 ($R^2 = 0.968$)	105
9	9	253 ($R^2 = 0.986$)	210
10	10·2.5MeCN	246 ($R^2 = 0.981$)	105

End group analysis by ^1H NMR spectroscopy indicated that the PCL possessed OR/OH end groups (e.g., Figure 12). Furthermore, the MALDI-TOF mass spectra (e.g., Figure 13) revealed the presence of both linear and cyclic products. For the ^1H NMR spectra and MALDI-TOF spectra of the PCL resulting from the use of **1–7**, **9** and **10**, see Figures S12–S29 in the Supporting Information.

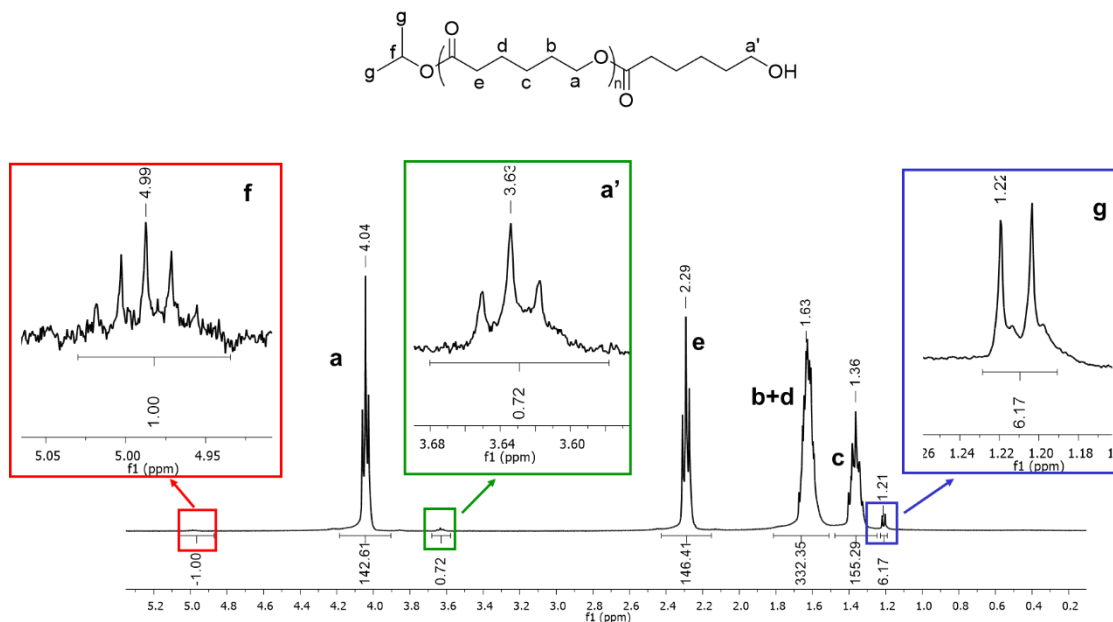


Figure 12. ^1H NMR spectrum (CDCl_3 , 400 MHz) of PCL prepared using **8** (Table 1, entry 8).

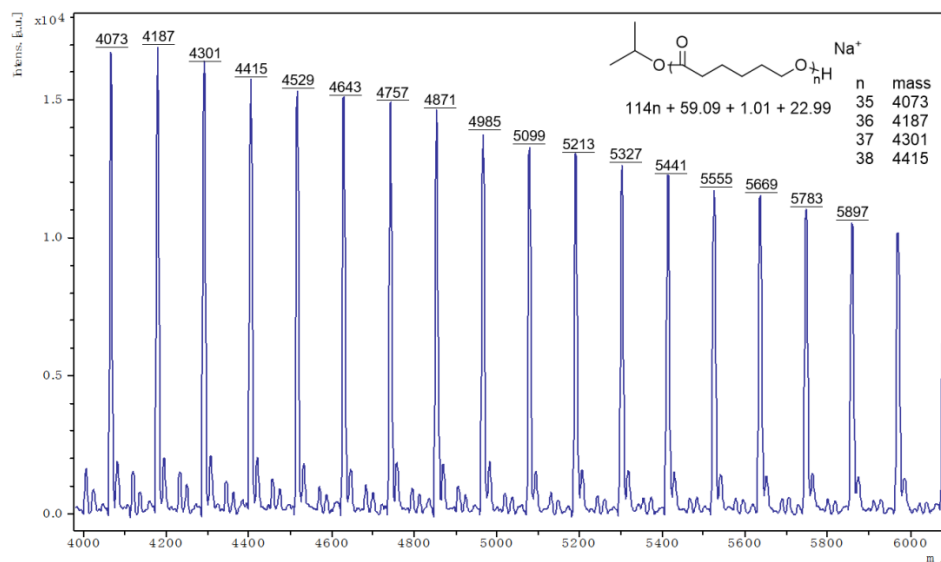


Figure 13. MALDI-TOF mass spectrum of PCL prepared using **8** (Table 1, entry 8).

2.3. Ring Opening Polymerization Studies of Rac-Lactide (*r*-LA)

Complexes **1–10** were screened as initiators in the ROP of *r*-LA at 130 °C using a monomer to Ti ratio of 250:1 (Table 3) under an N_2 atmosphere, unless stated otherwise. The L^1H_2 -derived complexes **1–5** exhibited good activities (72–98% conversion over 24 h at 130 °C; Table 3, entries 1–5). Indeed, even complex **2**, which bears only chelate ligands, exhibited a reasonable conversion at 78% (Table 3, entry 2). By contrast, the L^2H_3 -derived complexes **6** and **8–10** exhibited inferior conversions (28–65%; Table 3, entries 6, 8–10), suggesting the presence of the L^2H_3 -derived ligand set was less beneficial in terms of

accessing a high activity system for the ROP of *r*-LA. That said, the L²H₃-derived complex **7** proved to be the exception, and afforded a conversion of 98% (Table 3, entry 7). The alkoxide group effect on the ROP of *r*-LA is best illustrated by looking at the pairs of nearly identical structures, namely, **7** (*On*Pr) versus **8** (*Oi*Pr) and **9** (*Oi*Pr) versus **10** (*Ot*Bu) (Table 3, entries 7–10). For **7** and **8**, the use of *On*Pr appears to be far more favorable than *Oi*Pr, with conversions of 98 and 52%, respectively; using **7** (*On*Pr) also afforded a higher-molecular weight product (30 versus 14 kDa, respectively); **8** exhibited slightly better control. For **9** and **10**, the performance of the *Oi*Pr exceeded that of the *Ot*Bu derivative **10**, with **9** affording higher conversion (44 vs. 28%) and better control (1.15 vs. 1.37). These results, particularly the induction periods, may well reflect the steric bulk of alkoxide groups present, for example the bulkier *Ot*Bu group may hinder the coordination of *r*-LA to the Ti metal center. Comparison of the complexes **3** and **4**, which bear the same type of alkoxide group, suggests that the number of L¹H[−] ligands present may also be an important factor (Table 3, entries 3–4). However, the wide variety of structures afforded during these reactions makes further analysis of structure/activity relationships somewhat problematic. With this in mind, we have again looked at the ROP behavior of the titanium alkoxides [Ti(OR)₄] (R = Me, *n*Pr, *i*Pr, *t*Bu) in order to investigate the effect of the absence of L¹H₂ and L²H₃ derived ligands on titanium under the same ROP conditions as employed for **1**–**10**. After 24 h, the sequence of conversion for the [Ti(OR)₄] complexes was found to be [Ti(*On*Pr)₄] ≈ [Ti(OMe)₄] > [Ti(*Ot*Bu)₄] > [Ti(*Oi*Pr)₄]. Similar to the ROP results for ε-CL, [Ti(*On*Pr)₄] exhibited superior activity (vs. **1**–**10**), but with less control over the polymerization process (Table 3, entry 16). Interestingly, if the ROP of *r*-LA was conducted for only 90 min at 130 °C, then the observed conversions yielded the order [Ti(*On*Pr)₄] (96%) > [Ti(*Oi*Pr)₄] (80%) > [Ti(*Ot*Bu)₄] (8%) > [Ti(OMe)₄] (no conversion).

Table 3. ROP of *r*-LA catalyzed by Ti complexes **1**–**10** and [Ti(OR)₄].

Run	Catalyst	L ¹ /L ²	OR Group	LA:Ti	T (°C)	Conv. ^a (%)	M _n (calc.) ^b (kDa)	M _n (obs.) ^{c,d} (kDa)	Đ ^c	Pi ^e
1	1		OMe	250:1	130	90	32.0	22.0	1.34	0.39
2	2·MeCN		-	250:1	130	78	28.0	14.0	1.22	0.47
3	3	L ¹	<i>Oi</i> Pr	250:1	130	92	33.0	13.0	1.15	0.46
4	4·MeCN		<i>Oi</i> Pr	250:1	130	98	35.0	16.0	1.19	0.49
5	5·MeCN		<i>Ot</i> Bu	250:1	130	72	26.0	13.0	1.72	0.48
6	6·2.5MeCN		OMe	250:1	130	65	23.0	11.0	1.21	0.26
7	7·MeCN		<i>On</i> Pr	250:1	130	98	35.0	30.0	1.29	0.49
8	8		<i>Oi</i> Pr	250:1	130	52	19.0	14.0	1.19	0.46
9	9	L ²	<i>Oi</i> Pr	250:1	130	44	16.0	8.0	1.15	0.51
10	10·2MeCN		<i>Ot</i> Bu	250:1	130	28	10.0	12.0	1.37	0.16
11 ^f	4·MeCN		<i>Oi</i> Pr	250:1	130	20	7.3	4.6	1.18	-
12 ^f	7·MeCN		<i>On</i> Pr	250:1	130	16	5.8	3.6	1.10	-
15			OMe	250:1	130	99	35.7	0.5	1.24	-
16	[Ti(OR) ₄]		<i>On</i> Pr	250:1	130	99	35.7	0.7	3.03	-
17			<i>Oi</i> Pr	250:1	130	86	31.0	0.5	2.75	-
18			<i>Ot</i> Bu	250:1	130	98	35.4	1.7	2.60	-

Reaction conditions: *r*-LA 4.5 mmol, toluene 2 mL, 24 h, N₂ atmosphere. ^a Determined by ¹H NMR spectroscopy of the crude reaction mixture. ^b Calculated from [*r*-LA]/[Ti] × Conv. × M_w(LA) + M_w(end group). ^c From GPC. ^d Values corrected considering Mark–Houwink factor (0.58) from polystyrene standards in THF. ^e Pi = 1–2I_{isi}. ^f Reaction conducted in air.

The air stability of complexes **4** and **7** was also examined; they were employed to initiate the polymerization of *r*-LA at 130 °C with a [LA]:[Ti] ratio of 250:1 in air. Both complexes proved to be less active in air, with dramatically decreased conversions (Table 3, entries 11–12), and the M_n values were found to be lower than the calculated values.

The kinetics for the ROP of *r*-LA using **1**–**10** were investigated by in situ ¹H NMR spectroscopy studies, based on the relative areas of the methine signals of PLA and *r*-LA (5.06

and 4.18 ppm, respectively); see the Supporting Information, Figure S30 (displays results using **7**, Table 3, entry 7). The corresponding kinetics semi-logarithmic plots for **1–9** are shown in Figure 14 (data for **10** could not be recorded due to the slow reactivity of the complex). The apparent rate constant of **1–9** follows the trend $4 > 7 > 3 > 1 > 2 > 5 > 6 > 8 > 9$. The first order kinetic plot of *r*-LA polymerization using **6**, **8** and **9** showed an induction period of 300–400 min, suggesting the slow insertion of the LA unit because of the different nucleophilicity of the alkoxide groups [54]. The linearity of the plots using **1–5** and **7** indicates the absence of an induction period, and the ROP rate exhibits first order dependence on monomer concentration.

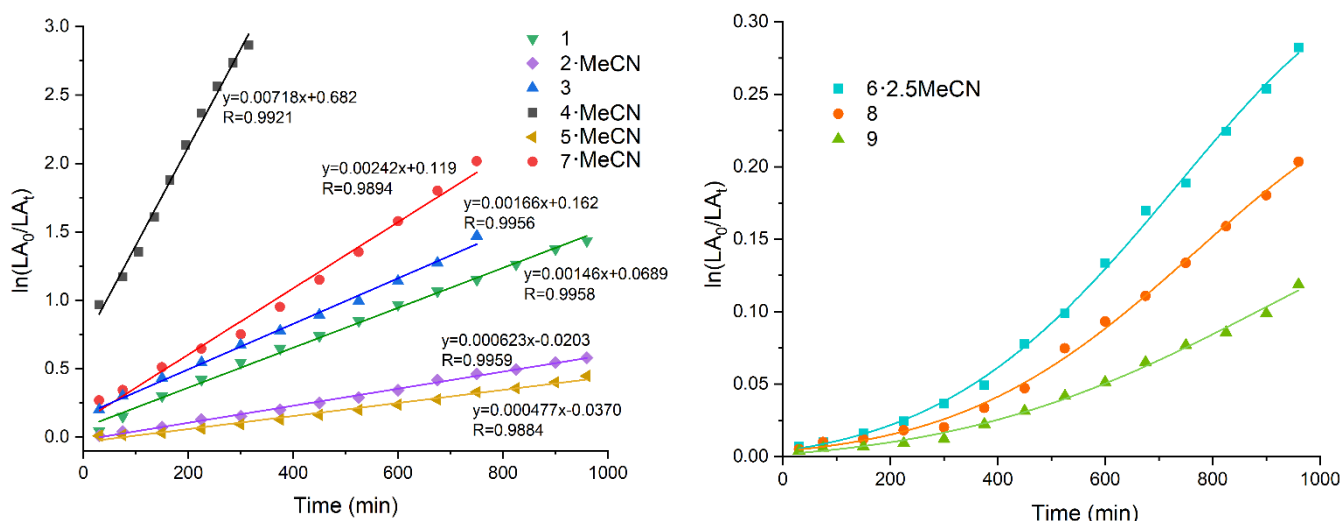


Figure 14. Semi-log plot of $\ln(LA_0/LA_t)$ versus time for ROP using complexes **1–5**, **7** (Left), **6** and **8–9** (Right) (Table 3, entries 1–9).

^1H NMR spectroscopy analysis of the end groups of the PLA synthesized with complex **10** indicated the presence of *tert*-butoxy and a hydroxyl chain terminus (Figure 15), suggesting that polymer initiation occurs through the insertion of lactide into the Ti–O bond via the coordination insertion mechanism. This is further supported by MALDI-TOF mass spectra (e.g., Figure 16). The major set of peaks with a mass difference of $m/z = 114$ Da corresponds to $144.15n + 72.11 + 1.01$, and is attributed to $(LA)_n + t\text{BuOH}$. A minor set of peaks corresponds to cyclic polymers separated by 144 Da. For the ^1H NMR spectra and MALDI-TOF spectra of the PLA resulting from the use of **1–5** and **7–9**, see Figures S31–S44 in the Supporting Information.

The stereochemical microstructure analysis of PDLLA was verified by the inspection of the methine region of ^{13}C NMR of the polymers (Figures S45–S49, Supporting Information). The methine carbon signal in the repeat unit of PLA is sensitive to the tetrad. The degree of stereoselectivity is defined by the parameter P_i , which is the probability of forming a new *i*-dyad [55]. From Table 3, we see that P_i is mostly < 0.5 , which indicates mostly the formation of an isotactic product [56]. For **9**, the data suggest the formation of an atactic polymer ($P_i = 0.51$).

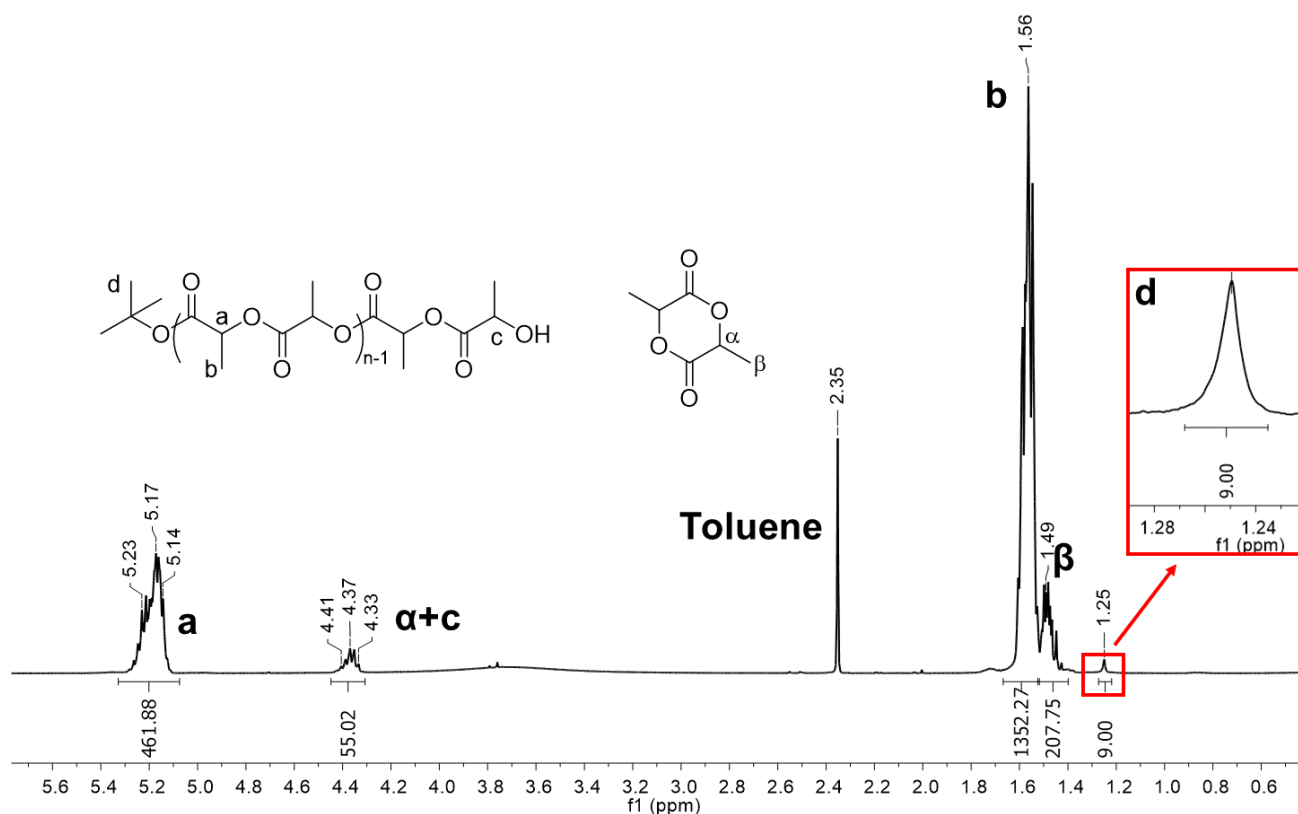


Figure 15. $^1\text{H NMR}$ (CDCl_3 , 400 MHz) spectrum of PLA prepared using 10·2MeCN (Table 3, entry 10).

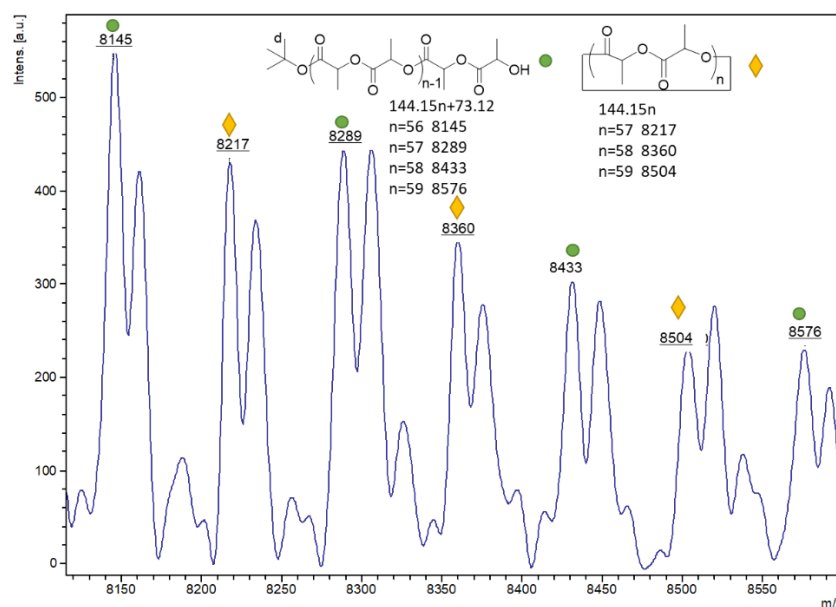


Figure 16. MALDI-TOF mass spectrum of PLA prepared using 10·2MeCN (Table 3, entry 10).

3. Materials and Methods

3.1. General

All reactions were conducted under an inert atmosphere using standard Schlenk techniques unless otherwise specified. Toluene was dried from sodium, acetonitrile was distilled from calcium hydride, and all solvents were degassed prior to use. IR spectra (nujol mulls, KBr windows) were recorded on a Nicolet Avatar 360 FTIR spectrometer; NMR spectrometer 400.2 MHz on a JEOL ECZ 400S spectrometer, with TMS $\delta_{\text{H}} = 0$ as

the internal standard or residual protic solvent [CD_3CN , $\delta\text{H} = 1.94$]. Chemical shifts are given in ppm (δ) and coupling constants (J) are given in Hertz (Hz). Elemental analyses were performed by the elemental analysis service at the Department of Chemistry, the University of Hull or OEA labs Ltd (UK). Matrix-Assisted Laser Desorption/Ionization Time of Flight (MALDI-TOF) mass spectrometry was performed in a Bruker autoflex III smart beam in linear mode, and the spectra were acquired by averaging at least 100 laser shots. 2,5-Dihydroxybenzoic acid was used as the matrix and THF as solvent. Sodium chloride was dissolved in methanol and used as the ionizing agent. Samples were prepared by mixing 20 μL of matrix solution in THF ($2 \text{ mg}\cdot\text{mL}^{-1}$) with 20 μL of matrix solution ($10 \text{ mg}\cdot\text{mL}^{-1}$) and 1 μL of a solution of ionizing agent ($1 \text{ mg}\cdot\text{mL}^{-1}$). Then 1 mL of these mixtures was deposited on a target plate and allowed to dry in air at ambient temperature. The metal alkoxides $[\text{Ti}(\text{OR})_4]$ (R = Me, *n*Pr, *i*Pr, *t*Bu) and the acids 2,2'-Ph₂C(X)(CO₂H) (X = OH, NH₂) were purchased from Sigma-Aldrich. Molecular weights were calculated from the experimental traces using the OmniSEC software.

3.2. Preparation of $[\text{Ti}_4(\text{L}^1)_2(\text{OMe})_{12}]$ (**1**)

In a 25 mL Schlenk tube under nitrogen, 2,2'-Ph₂C(OH)(CO₂H) (1.00 g, 4.38 mmol) was dissolved in dry toluene (20 mL), and two equivalent of $[\text{Ti}(\text{OMe})_4]$ (1.51 g, 8.76 mmol) was added into the reaction solution. The system was refluxed for 12 h, and following the removal of volatiles in vacuo, the residue was extracted in warm MeCN (12 mL), affording on prolonged standing in the refrigerator (5 °C) small, white crystals. Yield 50% (1.11 g). Anal. Calcd for $\text{C}_{40}\text{H}_{56}\text{O}_{18}\text{Ti}_4$ (1016.44 g/mol): C, 47.27; H, 5.55%; found: C, 47.07; H, 5.42%. HR-MS (EI): m/z 528.64 $[\text{Ti}_2\text{L}^1(\text{OMe})_6 - 3\text{H} + \text{Na}]^+$. ¹H NMR (400 MHz, Acetone-D₆) δ 7.76 (m, 8H, ArH), 7.30 (m, 4H, ArH), 7.18 (m, 6H, ArH), 7.09 (m, 2H, ArH), 4.65 (s, 6H, OMe), 4.52–4.48 (overlapping s, 6H OMe), 4.18 (s, 6H, OMe), 3.73 (m, 3H, OMe), 3.68 (s, 3H, OMe), 3.52 (overlapping s, 6H, OMe), 3.27 (s, 6H, OMe). IR (nujol mull, cm^{-1}): 2955(s), 2923(s), 2854(s), 2727(w), 2357(w), 1682(s), 1564(s), 1557(s), 1488(m), 1463(s), 1377(s), 1313(w), 1260(m), 1118(s), 1027(s), 916(w), 817(w), 801(w), 758(w), 722(m), 696(m), 666(w), 606(m), 505(m), 455(w).

3.3. Preparation of $[\text{Ti}(\text{L}^1\text{H})_3][\text{Ti}(\text{L}^1\text{H})(\text{L}^1\text{H})_2] \text{MeCN}$ (**2**·MeCN)

The synthesis of **2** was carried out according to the same procedure as for **1**, but using L^1H_2 (2.00 g, 8.76 mmol) and $[\text{Ti}(\text{OnPr})_4]$ (1.21 mL, 4.38 mmol). Yield 70% (2.24 g). Anal. Calcd for $\text{C}_{86}\text{H}_{67}\text{NO}_{18}\text{Ti}_2$ (1498.20 g/mol): C, 68.95; H, 4.51; N, 0.93%; found: C, 68.66; H, 4.75; N, 0.97%. HR-MS (EI): m/z 729.41 $[\text{Ti}(\text{L}^1\text{H})_3]^+$. ¹H NMR (400 MHz, CD₃CN, 25 °C): δ 7.74 (m, 2H, ArH), 7.61 (m, 1H, ArH), 7.51 (m, 2H, ArH), 7.40–7.20 (overlapping m, 25H, ArH); OH not observed. IR (nujol mull, cm^{-1}): 2957(s), 2923(s), 2953(s), 2359(w), 2340(w), 1596(w), 1457(m), 1376(m), 1260(m), 1090(s), 1020(s), 914(w), 866(w), 799(s), 720(w), 692(w), 668(w), 638(w), 608(w), 552(w), 467(w).

3.4. Preparation of $[\text{Ti}_4\text{O}(\text{L}^1)_2(\text{OiPr})_{10}]$ (**3**)

The synthesis of **3** was carried out according to the same procedure as for **1**, but using L^1H_2 (2.00 g, 8.76 mmol) and $[\text{Ti}(\text{OiPr})_4]$ (3.99 mL, 13.48 mmol). Yield 30% (1.26 g). Anal. Calcd for $\text{C}_{58}\text{H}_{90}\text{O}_{17}\text{Ti}_4$ (1250.89 g/mol): C, 55.69; H, 7.25%; found: C, 56.10; H, 7.22%. HR-MS (E/I): m/z 1256.84 $[\text{Ti}_4\text{O}(\text{L}^1)_2(\text{OiPr})_{10} + 6\text{H}]^+$. ¹H NMR (400 MHz, Acetone-D₆, 25 °C): δ 7.83–6.80 (bm, 20H, ArH), 3.86 (sept, $J = 6.0 \text{ Hz}$, 10H, CHMe₂), 1.07 (d, $J = 6.0 \text{ Hz}$, 60H, CHMe₂). IR (nujol mull, cm^{-1}): 2956(s), 2923(s), 2853(s), 1729(m), 1634(s), 1597(s), 1460(s), 1377(s), 1261(s), 1212(m), 1165(s), 1113(s), 1089(m), 1055(s), 1019(s), 1006(m), 941(m), 914(w), 854(m), 803(s), 777 (m), 757(m), 738(w), 722(s), 694(m), 661(w), 623(s), 612(s), 550(m), 527(w), 484(w), 467(w), 430(w).

3.5. Preparation of $[\text{Ti}_4\text{O}(\text{L}^1)_3(\text{OiPr})_8]$ (**4**·MeCN)

The synthesis of **4** was carried out according to the same procedure as for **1**, but using L^1H_2 (2.00 g, 8.76 mmol) and $[\text{Ti}(\text{OiPr})_4]$ (2.66 mL, 8.98 mmol). Yield 45% (1.42 g). Anal.

Calcd for $C_{66}H_{86}O_{18}Ti_4$ (1358.94 g/mol): C, 58.34; H, 6.38%; found: C, 57.89; H, 6.16%. HR-MS (EI): m/z 1272.71 $[Ti_2O(L^1)_3(OiPr)_7-2(iPr)]^+$, 1256.80 $[Ti_2O(L^1)_3(OiPr)_7-(OiPr)-(iPr)]^+$. 1H NMR (400 MHz, Acetone- D_6 , 25 °C): δ 7.83–6.67 (bm, 30H, ArH), 3.86 (sept, $J = 6.4$ Hz, 8H, $CHMe_2$), 1.07 (d, $J = 6.4$ Hz, 48H, $CHMe_2$). IR (KBr disc, cm^{-1}): 2955(s), 2923(s), 2853(s), 1961(w), 1887(w), 1821(w), 1728(m), 1633(m), 1957(m), 1491(m), 1462(s), 1377(s), 1261(m), 1211(m), 1165(m), 1110(s), 1088(m), 1045(s), 1025(s), 1006(m), 941(w), 913(w), 854(m), 803(s), 757(m), 738(w), 722(m), 694(m), 661(w), 622(w), 607(m), 538(m), 526(m), 485(w), 429(w).

3.6. Preparation of $[Ti_3(L^1)_4(OtBu)_4(CH_3CN)]$ (5· CH_3CN)

The synthesis of **5** was carried out according to the same procedure as for **1**, but using L^1H_2 (2.00 g, 8.76 mmol) and $[Ti(OtBu)_4]$ (3.38 mL, 8.75 mmol). Yield 10% (0.42 g). Anal. Calcd for $C_{74}H_{79}NO_{16}Ti_3$ (1382.04 g/mol): C, 64.31; H, 5.76; N, 1.01%; found: C, 63.94; H, 5.77; N, 0.94%. HR-MS (EI): m/z 1468.42 $[Ti_3(L^1)_4(OtBu)_4(CH_3CN)\cdot CH_3CN + 2Na]^+$. 1H -NMR (400 MHz, Acetone- D_6) δ 7.77–7.10 (bm, 40H, ArH), 2.28 (s, 3H, $MeCN$), 1.15 (s, 36H, $C(CH_3)_3$). IR (nujol mull, cm^{-1}): 2958(s), 2853(s), 2727(w), 2671(w), 1704(w), 1660(w), 1644(w), 1568(w), 1463(s), 1377(s), 1310(m), 1261(s), 1236(s), 1170(s), 1088(s), 1026(s), 941(w), 915(w), 795(s), 722(s), 694(m), 666(w), 638(w), 621(w), 607(m), 587(w), 545(m), 490(m), 456(w).

3.7. Preparation of $[Ti(L^2H_2)_3OMe]\cdot 2.5CH_3CN$ (6· $2.5CH_3CN$)

As for **1**, but using L^2H_3 (1.00 g, 4.40 mmol) and $[Ti(OMe)_4]$ (0.38 g, 2.21 mmol), affording **6·2.5CH₃CN** as colorless prisms. Yield 24% (0.46 g). Anal. Calcd for $C_{43}H_{39}N_3O_7Ti$ (860.30 g/mol): C, 68.17; H, 5.19; N, 5.55%; found: C, 67.98; H, 4.99; N, 5.46%. HR-MS (EI): m/z 1031.87 $[2 \times Ti(L^2H_2)_6(OMe)_2 - OMe - 2(L^2H_2)]$. 1H NMR (400 MHz, Acetone- D_6) δ 7.77–7.15 (bm, 30H, ArH), 3.27 (s, 3H, OMe), 2.95 (bs, 6H, NH_2). IR (KBr disc, cm^{-1}): 3336(w), 3246(w), 3056(m), 2958(s), 2923(s), 2854(s), 2360(w), 2342(w), 2250(w), 1682(s), 1651(w), 1589(m), 1494(m), 1463(s), 1448(s), 1377(s), 1261(s), 1191(w), 1101(s), 1019(s), 800(s), 764(m), 698(s), 677(w), 614(w), 583(w), 502(w), 455(w).

3.8. Preparation of $[Ti(L^2H_2)_2(OnPr)_6]\cdot CH_3CN$ (7· CH_3CN)

As for **1**, but using L^2H_3 (2.00 g, 8.80 mmol) and $[Ti(OnPr)_4]$ (2.61 mL, 8.80 mmol), affording **7·CH₃CN** as colorless prisms. Yield 80% (3.17 g). Anal. Calcd for $C_{46}H_{66}N_2O_{10}Ti_2$ (902.77 g/mol): C, 61.20; H, 7.37; N, 3.10%; found: C, 60.93; H, 7.02; N, 2.98%. HR-MS (EI): m/z 811.76 $[Ti_2(L^2H_2)_2(OnPr)_6 - 2nPr - 3H^+]$. 1H NMR (400 MHz, CD_3CN , 25 °C): 7.40 (overlapping m, 5H, ArH), 7.33 (overlapping m, 13H, ArH), 7.23 (overlapping m, 2H, ArH), 4.45–3.99 (overlapping bm, 12H, $NH_2 + 5x OCH_2CH_2CH_3$), 3.43 (m, $J = 6.4$ Hz, 2H, $OCH_2CH_2CH_3$), 2.31 (bs, 2H, NH_2), 1.46 (overlapping m, 12H, $OCH_2CH_2CH_3$), 0.89–0.62 (overlapping m, 18H, $OCH_2CH_2CH_3$). IR (KBr disc, cm^{-1}): 3336(w), 3246(w), 3056(m), 2958(s), 2923(s), 2854(s), 2360(w), 2342(w), 2250(w), 1682(s), 1651(w), 1589(m), 1494(m), 1463(s), 1448(s), 1377(s), 1261(s), 1191(w), 1101(s), 1019(s), 800(s), 764(m), 698(s), 677(w), 614(w), 583(w), 502(w), 455(w).

3.9. Preparation of $[Ti_2(L^2H_2)_2(OiPr)_6]$ (8)

As for **1**, but using L^2H_3 (2.00 g, 8.76 mmol) and $[Ti(OiPr)_4]$ (2.61 mL, 8.80 mmol), affording **8** as colorless prisms. Yield 30% (0.40 g). Anal. Calcd for $C_{46}H_{66}N_2O_{10}Ti_2$ (902.88 g/mol): C, 61.20; H, 7.37; N, 3.10%; Found: C, 60.12; H, 6.92; N, 3.38%. HR-MS (EI): m/z 1080.09 = $2[Ti_2(L^2H_2)_2(OiPr)_6] - 3(L^2H_2) - iPr - 3H^+$. 1H -NMR (400 MHz, Acetone- D_6): δ 7.31 (overlapping m, 8H, ArH), 7.26 (overlapping m, 12H, ArH), 5.01 (sept, $J = 6.4$ Hz, 2H, $CH(CH_3)_2$), 3.86 (sept, $J = 6.4$ Hz, 4H, $CH(CH_3)_2$), 3.27 (bs, 2H, NH_2), 2.86 (bs, 2H, NH_2), 1.16 (d, $J = 6.4$ Hz, 12H, $CH(CH_3)_2$), 1.08 (d, $J = 6.4$ Hz, 24H, $CH(CH_3)_2$). IR (KBr disc, cm^{-1}): 3366(m), 3296(m), 2955(s), 2923(s), 2853(s), 2724(w), 2613(w), 2355(w), 1986(w), 1960(w), 1900(w), 1682(s), 1651(m), 1633(m), 1574(m), 1495(m), 1463(s), 1378(s), 1365(m), 1322(m), 1261(s), 1192(w), 1160(m), 1105 (s), 1073(m), 1014(s), 980(m), 948(w),

932(m), 916(w), 851(m), 801(s), 775(w), 758(w), 732(w), 700(m), 674(w), 624(m), 606(m), 553(m), 524(w), 499(m), 472(m), 458(m), 426(w).

3.10. Preparation of $[(L^2H_2)_2Ti(OiPr)_2]$ (**9**)

As for **1**, but using L^2H_3 (2.00 g, 8.76 mmol) and $[Ti(OiPr)_4]$ (1.31 mL, 4.40 mmol), affording **9** as colorless prisms. Yield 30% (0.82 g). Anal. Calcd for $3 \times [C_{34}H_{38}N_2O_6Ti]$ (1855.69 g/mol): C, 66.02; H, 6.19; N, 4.53%; found: C, 65.88; H, 6.07; N, 4.42%. HR-MS (EI): m/z 770.16 = $2 \times [Ti(L^2H_2)_2(OiPr)_2] - 2L^2H_2 - CH_3$. 1H -NMR (400 MHz, $CDCl_3$): δ 7.31–6.87 (2x bm, 20H, ArH), 4.65 (sept, $J = 6.4$ Hz, 2H, $CHMe_2$), 3.70 (bs, 4H, NH_2), 1.19 (d, $J = 6.4$ Hz, 12H, $CHMe_2$). IR (nujol mull, cm^{-1}): 3356(w), 3316(w), 3280(w), 3202(w), 3134(w), 2955(s), 2923(s), 2853(s), 1667(s), 1573(m), 1494(w), 1463(s), 1377(s), 1344(w), 1307(m), 1261(m), 1192(w), 1165(w), 1117(m), 1066(w), 1050(w), 1017(m), 967(w), 922(w), 911(w), 892(w), 857(m), 819(s), 802(s), 763(w), 747(m), 723(m), 696(m), 676(w), 631(w), 617(w), 561(w), 540(w), 517(w), 492(w), 458(m), 405(m).

3.11. Preparation of $[(L^2H_2)_2Ti(OtBu)_2] \cdot 2MeCN$ (**10**·2MeCN)

As for **1**, but using L^2H_3 (2.00 g, 8.76 mmol) and $[Ti(OtBu)_4]$ (3.00 mL, 8.80 mmol), affording **10**·2MeCN as colorless prisms. Yield 60% (3.85 g). Anal. Calcd for $C_{36}H_{42}N_2O_6Ti \cdot 2[CH_3CN]$ (728.72 g/mol): C, 65.93; H, 6.64; N, 7.69%; found: C, 65.40; H, 6.74; N, 6.98%. HR-MS (EI): m/z 589.781 $[Ti(L^2H_2)_2(OtBu)_2 - tBu]$. 1H -NMR (400 MHz, Acetone- D_6) δ 7.54 (bm, 2H, ArH), 7.47 (bm, 2H, ArH), 7.36 (bm, 4H, ArH), 7.29 (overlapping m, 8H, ArH), 7.18 (bm, 4H, ArH), 4.43 (bs, 2H, NH_2), 1.16 (s, 18H, $C(CH_3)_3$), 1.03 (bs, 2H, NH_2). IR (nujol mull, cm^{-1}): 3347(m), 3244(m), 3057(w), 2955(s), 2922(s), 2853(s), 2727(w), 2671(w), 1684(s), 1651(s), 1572(s), 1494(m), 1463(s), 1377(s), 1362(m), 1327(m), 1296(s), 1261(m), 1234(m), 1182(s), 1124(s), 1078(m), 1032(w), 1015(s), 990(s), 861(w), 821(m), 793(m), 767(m), 758(m), 737(w), 723(w), 699(s), 677(m), 624(m), 609(m), 579(m), 544(w), 522(w), 489(m), 466(m), 447(w), 421(w).

3.12. ROP of ϵ -Caprolactone or Rac-Lactide

All polymerizations were carried out in Schlenk tubes under nitrogen atmosphere. ϵ -CL and *r*-LA were polymerized using complexes and toluene as solvent (2 mL). The reaction mixture was then placed into a preheated oil bath to the required temperature (shown in Tables 1 and 3). The reaction was quenched by the addition of an excess of glacial acetic acid (0.2 mL), then the reaction solution was poured into cold methanol (20 mL). The precipitated polymers were recovered by filtration, washed with methanol and dried at 60 °C overnight in a vacuum oven.

3.13. Crystallography

Full sets of X-ray diffraction intensity data were collected using modern X-ray diffractometers at the National Crystallography Service in Southampton, UK. The routine processing of raw intensity data and multi-scan absorptions corrections were applied. The structures were solved using dual-space methods within SHELXT and full-matrix least squares refinement was carried out using SHELXL-2018 [57] via the program Olex2. [58] All non-hydrogen positions were located in direct and difference Fourier maps and refined using anisotropic displacement parameters. Disorder was modeled conservatively using standard techniques.

4. Conclusions

We have investigated the reaction between acids of the type 2,2'- $Ph_2C(X)(CO_2H)$, where $X = OH$ and NH_2 , i.e., benzoic acid (2,2'-diphenylglycolic acid, L^1H_2), and 2,2'-diphenylglycine (L^2H_3), with titanium tetraalkoxides $[Ti(OR)_4]$ ($R = Me, nPr, iPr, tBu$). The resulting mono-, bi-, tri or tetra-metallic products have been structurally characterized and employed as catalysts for the ROP of both ϵ -CL and *r*-LA. For the ROP of ϵ -CL, the complex $[Ti(L^2H_2)_2(OnPr)_6] \cdot CH_3CN$ (**7**· CH_3CN) exhibited the best performance, achieving

a conversion of $\geq 99\%$ within 6 min at 100 °C. A number of the other systems proved to be quite sluggish and experienced induction periods. For the ROP of *r*-LA, the benzoic acid-derived complexes all exhibited good conversions, whilst most of the 2,2'-diphenylglycine-derived species proved to be poorer catalysts. The exception again was complex 7, which achieved high conversion (98%). As well as polymers bearing alkoxide/hydroxy end groups, there was evidence of cyclic polymers.

Supplementary Materials: The following supporting information can be downloaded at <https://www.mdpi.com/article/10.3390/catal12090935/s1>. Figure S1. Harris notation and its application in describing these ligands. Figure S2. Alternative view of 1. Figure S3. Coordination about the two independent Ti ions in 2. Figure S4. Alternate view (ORTEP) of 3 with atoms drawn as 25% probability ellipsoids. Minor disorder and hydrogen atoms are omitted for clarity. Figure S5. Asymmetric unit of 4 with atoms drawn as spheres of arbitrary radius. Each disorder component is illustrated; hydrogen atoms are not shown for clarity. Figure S6. Alternative view of 5 with atoms drawn as 50% probability ellipsoids. For clarity hydrogen atoms have been omitted. Figure S7. View of the crystal structure of 6 down *a*. Dashed lines show hydrogen bonds. Figure S8. The two unique complexes in 7 composed of Ti1 and Ti2. Symmetry-equivalent atoms are generated by the following symmetry operations: $\$1 = 1 - x, 2 - y, 2 - z$; $\$2 = -x, 1 - y, 1 - z$. Figure S9. Two Ti cluster present in 8. Symmetry operation used to generate equivalent atoms: $i = 1 - x, 1 - y, 1 - z$. Figure S10. Asymmetric unit of 9. A portion of the infinite hydrogen bonded chain running parallel to the crystallographic *a* direction (left-right on the image) is shown as dashed lines. Figure S11. Hydrogen-bonded chain within 10. Dashed lines show hydrogen bonds. Figure S12. ^1H NMR (400 MHz, CDCl_3) spectrum of PCL using 1 (Table 1, entry 1). Figure S13. MALDI-TOF spectrum of PCL using 1 (Table 1, entry 1). Figure S14. ^1H NMR (400 MHz, CDCl_3) spectrum of PCL using 2 (Table 1, entry 2). Figure S15. MALDI-TOF spectrum of PCL using 2 (Table 1, entry 2). Figure S16. ^1H NMR (400 MHz, CDCl_3) spectrum of PCL using 3 (Table 1, entry 3). Figure S17. MALDI-TOF spectrum of PCL using 3 (Table 1, entry 3). Figure S18. ^1H NMR (400 MHz, CDCl_3) spectrum of PCL using 4 (Table 1, entry 4). Figure S19. MALDI-TOF spectrum of PCL using 4 (Table 1, entry 4). Figure S20. ^1H NMR (400 MHz, CDCl_3) spectrum of PCL using 5 (Table 1, entry 5). Figure S21. MALDI-TOF spectrum of PCL using 5 (Table 1, entry 5). Figure S22. ^1H NMR (400 MHz, CDCl_3) spectrum of PCL using 6 (Table 1, entry 6). Figure S23. MALDI-TOF spectrum of PCL using 6 (Table 1, entry 6). Figure S24. ^1H NMR (400 MHz, CDCl_3) spectrum of PCL using 7 (Table 1, entry 7). Figure S25. MALDI-TOF of PCL using 7 (Table 1, entry 7). Figure S26. ^1H NMR (400 MHz, CDCl_3) spectrum of PCL using 9 (Table 1, entry 9). Figure S27. MALDI-TOF of PCL using 9 (Table 1, entry 9). Figure S28. ^1H NMR (400 MHz, CDCl_3) spectrum of PCL using 10 (Table 1, entry 10). Figure S29. MALDI-TOF spectrum of PCL using 10 (Table 1, entry 10). Figure S30. 3D time-resolved ^1H NMR (400 MHz, toluene- d_8) of kinetics of *r*-LA using complex 7 (Table 3, entry 7). Figure S31. ^1H NMR (400 MHz, CDCl_3) spectrum of PLA using 1 (Table 3, entry 1). Figure S32. MALDI-TOF spectrum of PLA using 1 (Table 3, entry 1). Figure S33. ^1H NMR (400 MHz, CDCl_3) spectrum of PLA using 2 (Table 3, entry 2). Figure S34. MALDI-TOF spectrum of PLA using 2 (Table 3, entry 2). Figure S35. MALDI-TOF spectrum of PLA using 3 (Table 3, entry 3). Figure S36. ^1H NMR (400 MHz, CDCl_3) spectrum of PLA using 4 (Table 3, entry 4). Figure S37. MALDI-TOF spectrum of PLA using 4 (Table 3, entry 4). Figure S38. MALDI-TOF spectrum of PLA using 5 (Table 3, entry 5). Figure S39. ^1H NMR (400 MHz, CDCl_3) spectrum of PLA using 7 (Table 3, entry 7). Figure S40. MALDI-TOF spectrum of PLA using 7 (Table 3, entry 7). Figure S41. ^1H NMR (400 MHz, CDCl_3) spectrum of PLA using 8 (Table 3, entry 8). Figure S42. MALDI-TOF spectrum of PLA using 8 (Table 3, entry 8). Figure S43. ^1H NMR (400 MHz, CDCl_3) spectrum of PLA using 9 (Table 3, entry 9). Figure S44. MALDI-TOF spectrum of PLA using 9 (Table 3, entry 9). Figure S45. ^{13}C NMR spectrum of methine carbon in PLA using 1 (left) and 2 (right) (Table 3, entries 1 and 2). Figure S46. ^{13}C NMR spectrum of methine carbon in PLA using 3 (left) and 4 (right) (Table 3, entries 3 and 4). Figure S47. ^{13}C NMR spectrum of methine carbon in PLA using 5 (left) and 6 (right) (Table 3, entries 5 and 6). Figure S48. ^{13}C NMR spectrum of methine carbon in PLA using 7 (left) and 8 (right) (Table 3, entries 7 and 8). Figure S49. ^{13}C NMR spectrum of methine carbon in PLA using 9 (left) and 10 (right) (Table 3, entries 9 and 10). CCDC 2178997-2179006 contains the supplementary crystallographic data for this paper. These data can be obtained free of charge from The Cambridge Crystallographic Data Centre via www.ccdc.cam.ac.uk/data_request/cif.

Author Contributions: X.Z. conducted the investigation and original draft preparation; K.C. formal analysis; O.S. investigation; T.J.P. formal analysis. C.R. conceptualization; funding acquisition; supervision; writing review and editing. All authors have read and agreed to the published version of the manuscript.

Funding: This research was funded by the EPSRC, grant number EP/R023816/1.

Data Availability Statement: Not applicable.

Acknowledgments: X.Z. thanks the University of Hull for a studentship. We thank the EPSRC National Crystallographic Service at Southampton for data collection.

Conflicts of Interest: The authors declare no conflict of interest. The funders had no role in the design of the study; in the collection, analyses, or interpretation of data; in the writing of the manuscript, or in the decision to publish the results.

References

1. Kamar, N.E.; Jeong, W.; Waymouth, R.M.; Pratt, R.C.; Lohmeijer, B.G.G.; Hedrick, J.L. Organocatalytic Ring-Opening Polymerization. *Chem. Rev.* **2007**, *107*, 5813–5840. [[CrossRef](#)] [[PubMed](#)]
2. Williams, C.K.; Hillmyer, M.A. Polymers from Renewable Resources: A Perspective for a Special Issue of Polymer Reviews. *Polym. Rev.* **2008**, *48*, 1–10. [[CrossRef](#)]
3. Place, E.S.; George, J.H.; Williams, C.K.; Stevens, M.H. Synthetic Polymer Scaffolds for Tissue Engineering. *Chem. Soc. Rev.* **2009**, *38*, 1139–1151. [[CrossRef](#)] [[PubMed](#)]
4. Labet, M.; Thielemans, W. Synthesis of Polycaprolactone: A review. *Chem. Soc. Rev.* **2009**, *38*, 3484–3504. [[CrossRef](#)] [[PubMed](#)]
5. Arbaoui, A.; Redshaw, C. Metal Catalysts for ϵ -caprolactone polymerisation. *Polym. Chem.* **2010**, *1*, 801–826. [[CrossRef](#)]
6. Lecomte, P.; Jérôme, C. *Synthetic Biodegradable Polymers*; Rieger, B., Künkel, A., Coates, G., Reichardt, R., Dinjus, E., Zevaco, T., Eds.; Springer: Berlin/Heidelberg, Germany, 2011; Volume 245, pp. 173–211. ISBN -13:978-3642271533.
7. Redshaw, C. Use of Metal Catalysts Bearing Schiff-Base Macrocycles for the Ring Opening Polymerization (ROP) of Cyclic Esters. *Catalysts* **2017**, *7*, 165. [[CrossRef](#)]
8. Nifant'ev, I.; Ivchenko, P. Coordination Ring Opening Polymerization of Cyclic Esters: A Critical Overview of DFT Modeling and Visualization of the Reaction Mechanisms. *Molecules* **2019**, *24*, 4117. [[CrossRef](#)]
9. Lynbov, D.M.; Tolpygin, A.O.; Trifoner, A.A. Rare earth metal complexes as catalysts for ring opening polymerization of cyclic esters. *Coord. Chem. Rev.* **2019**, *392*, 83–145. [[CrossRef](#)]
10. Santoro, O.; Zhang, X.; Redshaw, C. Synthesis of Biodegradable Polymers: A Review on the use of Schiff-Base Metal Complexes as Catalysts for the Ring Opening Polymerization (ROP) of Cyclic Esters. *Catalysts* **2020**, *10*, 800. [[CrossRef](#)]
11. Gruszka, W.; Garden, J.A. Advances in heterometallic (co)polymerization catalysis. *Nat. Commun.* **2021**, *12*, 3252. [[CrossRef](#)]
12. Albertsson, A.-C.; Varma, I.K. Recent Developments in Ring Opening Polymerization of Lactones for Biomedical Applications. *Biomacromolecules* **2003**, *4*, 1466–1486. [[CrossRef](#)] [[PubMed](#)]
13. Tian, H.; Tang, Z.; Zhuang, X.; Chen, X.; Jing, X. Biodegradable Synthetic Polymers: Preparation, functionalization and biomedical application. *Prog. Polym. Sci.* **2012**, *37*, 237–280. [[CrossRef](#)]
14. Zhang, X.; Fevre, M.; Jones, G.O.; Waymouth, R.M. Catalysis as an Enabling Science for Sustainable Polymers. *Chem. Rev.* **2018**, *118*, 839–885. [[CrossRef](#)] [[PubMed](#)]
15. Redshaw, C. Metallocalixarene catalysts: α -olefin polymerization and ROP of cyclic esters. *Dalton Trans.* **2016**, *45*, 9018–9030. [[CrossRef](#)]
16. Jianming, R.; Anguo, X.; Hongwei, W.; Hailin, Y. Review—Recent development of ring-opening polymerization of cyclic esters using aluminum complexes. *Des. Monomers Polym.* **2014**, *17*, 345–355. [[CrossRef](#)]
17. Gao, J.; Zhu, D.; Zhang, W.; Solan, G.A.; Ma, Y.; Sun, W.-H. Recent progress in the application of group 1, 2 & 13 metal complexes as catalysts for the ring opening polymerization of cyclic esters. *Inorg. Chem. Front.* **2019**, *6*, 2619–2652. [[CrossRef](#)]
18. Santoro, O.; Redshaw, C. Use of Titanium Complexes Bearing Diphenolate or Calix[n]arene Ligands in α -Olefin Polymerization and the ROP of Cyclic Esters. *Catalysts* **2020**, *10*, 210. [[CrossRef](#)]
19. Stevels, W.M.; Ankoné, M.J.K.; Dijkstra, P.J.; Feijen, J. Kinetics and Mechanism of L-Lactide Polymerization Using Two Different Yttrium Alkoxides as Initiators. *Macromolecules* **1996**, *29*, 6132–6138. [[CrossRef](#)]
20. Simic, V.; Spassky, N.; Hubert-Pfalzgraf, L.G. Ring-Opening Polymerization of D,L-Lactide Using Rare-Earth μ -Oxo Isopropoxides as Initiator Systems. *Macromolecules* **1997**, *30*, 7338–7340. [[CrossRef](#)]
21. O'Keefe, B.J.; Monnier, S.M.; Hillmyer, M.A.; Tolman, W.B. Rapid and Controlled Polymerization of Lactide by Structurally Characterized Ferric Alkoxides. *J. Am. Chem. Soc.* **2001**, *123*, 339–340. [[CrossRef](#)]
22. Kim, Y.; Verkade, J.G. A Tetrameric Titanium Alkoxide as a Lactide Polymerization Catalyst. *Macromol. Rapid Commun.* **2002**, *23*, 917–921. [[CrossRef](#)]
23. Egevardt, C.; Giese, S.O.K.; Santos, A.D.d.C.; Barison, A.; de Sá, E.L.; Filho, A.Z.; da Silva, T.A.; Zawadzki, S.F.; Soares, J.F.; Nunes, G.G. ϵ -caprolactone and lactide polymerization promoted by an ionic titanium(IV)/iron(III) polynuclear halo-alkoxide. *J. Polym. Sci. A Polym. Chem.* **2014**, *52*, 2509–2517. [[CrossRef](#)]

24. Ryan, J.D.; Gagnon, K.J.; Teat, S.J.; McIntosh, R.D. Flexible macrocycles as versatile supports for catalytically active metal clusters. *Chem. Commun.* **2016**, *52*, 9071–9073. [[CrossRef](#)] [[PubMed](#)]
25. Cols, J.-M.E.P.; Taylor, C.E.; Gagnon, K.J.; Teat, S.J.; McIntosh, R.D. Well-defined Ti₄ pre-catalysts for the ring-opening polymerisation of lactide. *Dalton Trans.* **2016**, *45*, 17729–17738. [[CrossRef](#)]
26. Cols, J.M.E.P.; Hill, V.G.; Williams, S.K.; McIntosh, R.D. Aggregated initiators: Defining their role in the ROP of *rac*-lactide. *Dalton Trans.* **2018**, *47*, 10626–10635. [[CrossRef](#)]
27. Jenkins, D.T.; Fazekas, E.; Patterson, S.B.H.; Rosair, G.M.; Vilela, F.; McIntosh, R.D. Polymetallic Group 4 Complexes: Catalysts for the Ring Opening Polymerisation of *rac*-Lactide. *Catalysts* **2021**, *11*, 551. [[CrossRef](#)]
28. Braun, M. The “Magic” Diarylhydroxymethyl group. *Angew. Chem. Int. Ed.* **1996**, *35*, 519–522. [[CrossRef](#)]
29. Braun, M. The diaryl (oxy) methyl group: More than an innocent bystander in chiral auxiliaries, catalysts, and dopants. *Angew. Chem. Int. Ed.* **2012**, *51*, 2550–2562. [[CrossRef](#)]
30. Al-Khafaji, Y.; Elsegood, M.R.J.; Frese, J.W.A.; Redshaw, C. Ring opening polymerization of lactides and lactones by multimetallic alkyl zinc complexes derived from the acids Ph₂C(X)CO₂H (X = OH, NH₂). *RSC Adv.* **2017**, *7*, 4510–4517. [[CrossRef](#)]
31. Wang, X.; Zhao, K.-Q.; Mo, S.; Al-Khafaji, Y.; Prior, T.J.; Elsegood, M.R.J.; Redshaw, C. Organoaluminium Complexes Derived from Anilines or Schiff Bases for the Ring-Opening Polymerization of ϵ -Caprolactone, δ -Valerolactone and *rac*-Lactide. *Eur. J. Inorg. Chem.* **2017**, *2017*, 1951–1965. [[CrossRef](#)]
32. Al-Khafaji, Y.F.; Prior, T.J.; Horsburgh, L.; Elsegood, M.R.J.; Redshaw, C. Multimetallic Lithium Complexes Derived from the Acids Ph₂C(X)CO₂H (X = OH, NH₂): Synthesis, Structure and Ring Opening Polymerization of Lactides and Lactones. *Chem. Select* **2017**, *2*, 759–768. [[CrossRef](#)]
33. Collins, J.; Santoro, O.; Prior, T.J.; Chen, K.; Redshaw, C. Rare-earth metal complexes derived from the acids Ph₂C(X)CO₂H (X = OH, NH₂): Structural and ring opening polymerization (ROP) studies. *J. Mol. Struct.* **2021**, *1224*, 129083. [[CrossRef](#)]
34. Zhang, X.; Prior, T.J.; Redshaw, C. Niobium and Tantalum complexes derived from the acids Ph₂C(X)CO₂H (X = OH, NH₂): Synthesis, structure and ROP capability. *New J. Chem.* **2022**, *46*, 14146–14154. [[CrossRef](#)]
35. Alshamrani, A.F.A.; Santoro, O.; Ounsworth, S.; Prior, T.J.; Stasiuk, G.J.; Redshaw, C. Synthesis, characterisation and ROP catalytic evaluation of Cu(II) complexes bearing 2,2'-diphenylglycine-derived moieties. *Polyhedron* **2021**, *195*, 114977. [[CrossRef](#)]
36. Gibson, V.C.; Redshaw, C.; Clegg, W.; Elsegood, M.R.J. Synthesis and characterisation of molybdenum complexes bearing highly functionalised imido substituents. *Dalton Trans.* **1997**, *18*, 3207–3212. [[CrossRef](#)]
37. Redshaw, C.; Gibson, V.C.; Clegg, W.; Edwards, A.J.; Miles, B. Pentamethylcyclopentadienyl tungsten complexes containing imido, hydrazido and amino acid derived N-O chelate ligands. *Dalton Trans.* **1997**, *18*, 3343–3347. [[CrossRef](#)]
38. Redshaw, C.; Elsegood, M.R.J.; Holmes, K.E. Synthesis of hexa- and dodecanuclear organoaluminum ring structures incorporating the “magic” Ph₂C(X) Group (X = O⁻, NH⁻). *Angew. Chem. Int. Ed.* **2005**, *44*, 1850–1853. [[CrossRef](#)]
39. Redshaw, C.; Elsegood, M.R.J. Synthesis of Tetra-, Hexa-, and Octanuclear Organozinc Ring Systems. *Angew. Chem. Int. Ed.* **2007**, *119*, 7453–7457. [[CrossRef](#)]
40. Arbaoui, A.; Redshaw, C.; Hughes, D.L.; Elsegood, M.R.J. Arylboron complexes of the acids Ph₂C(XH)CO₂H (X = O, NH). *Inorg. Chim. Acta* **2009**, *362*, 509–514. [[CrossRef](#)]
41. Thielemann, D.T.; Wagner, A.T.; Lan, Y.; Anson, C.E.; Gamer, M.T.; Powell, A.K.; Roesky, P.W. Slow magnetic relaxation in four square-based pyramidal dysprosium hydroxo clusters ligated by chiral amino acid anions—A comparative study. *Dalton Trans.* **2013**, *42*, 14794–14800. [[CrossRef](#)]
42. Alshamrani, A.F.; Prior, T.J.; Burke, B.P.; Roberts, D.P.; Archibald, S.J.; Stasiuk, G.; Higham, L.J.; Redshaw, C. Water-soluble rhenium phosphine complexes incorporating the Ph₂C(X) motif (X = O⁻, NH⁻): Structural and Cytotoxicity studies. *Inorg. Chem.* **2020**, *59*, 2367–2378. [[CrossRef](#)] [[PubMed](#)]
43. Le Roux, E. Recent advances on tailor-made titanium catalysts for biopolymer synthesis. *Coord. Chem. Rev.* **2016**, *306*, 65–85. [[CrossRef](#)]
44. Webster, R.L. Random copolymerisations catalysed by simple titanium α -amino acid complexes. *RSC Adv.* **2014**, *4*, 5254–5260. [[CrossRef](#)]
45. Bermejo, E.; Carballo, R.; Castiñeiras, A.; Lago, A.B. Coordination of α -hydroxycarboxylic acids with first-row transition ions. *Coord. Chem. Rev.* **2013**, *257*, 2639–2651. [[CrossRef](#)]
46. At the Time of Writing (18.6.22), the Price of 100 g of Benzilic acid Costs £17.90 + VAT (from Merck/Sigma Aldrich). Available online: <https://www.sigmaaldrich.com/GB/en/substance/benzilicacid2282476937> (accessed on 18 June 2022).
47. Coxall, R.A.; Harris, S.G.; Henderson, D.K.; Parsons, S.; Tasker, P.A.; Winpenney, R.E.P. Inter-ligand reactions: In situ formation of new polydentate ligands. *J. Chem. Soc. Dalton Trans.* **2000**, *14*, 2349–2356. [[CrossRef](#)]
48. Kemmitt, T.; Gainsford, G.J.; Al-Salim, N.I. An oxo-bridged centrosymmetric tetranuclear titanium compound. *Acta Cryst. Sect. C* **2004**, *60*, m42–m43. [[CrossRef](#)]
49. At the Time of Writing (18.6.22), the Price of 5 g of 2,2'-Diphenylglycine Costs £104.00 + VAT (from Merck/Sigma Aldrich). Available online: <https://www.sigmaaldrich.com/GB/en/product/aldrich/161918> (accessed on 18 June 2022).
50. Baško, M.; Kubisa, P. Cationic copolymerization of ϵ -caprolactone and L,L-lactide by an activated monomer mechanism. *J. Polym. Sci. Part A Polym. Chem.* **2006**, *44*, 7071–7081. [[CrossRef](#)]

51. Delcroix, D.; Couffin, A.; Susperregui, N.; Navarro, C.; Maron, L.; Martin-Vaca, B.; Bourissou, D. Phosphoric and phosphoramidic acids as bifunctional catalysts for the ring-opening polymerization of ϵ -caprolactone: A combined experimental and theoretical study. *Polym. Chem.* **2011**, *2*, 2249–2256. [[CrossRef](#)]
52. Wright, D.A.; Williams, D.A. The Crystal and Molecular Structure of Titanium Methoxide. *Acta Cryst.* **1968**, *B24*, 1107–1114. [[CrossRef](#)]
53. Martin, R.L.; Winter, G. Structure of the Trinuclear Titanium(IV) Alkoxides. *Nature* **1960**, *188*, 313–315. [[CrossRef](#)]
54. Cui, Y.; Chen, C.; Sun, Y.; Wu, J.; Pan, X. Ioselective mechanism of the ring-opening polymerization of *rac*-lactide catalyzed by chiral potassium binolates. *Inorg. Chem. Front.* **2017**, *4*, 261–269. [[CrossRef](#)]
55. Zhong, Z.; Dijkstra, P.J.; Feijen, J. Controlled and stereoselective polymerization of lactide: Kinetics, selectivity, and microstructures. *J. Am. Chem. Soc.* **2003**, *125*, 11291–11298. [[CrossRef](#)] [[PubMed](#)]
56. Li, H.; Wang, C.; Bai, F.; Yue, J.; Woo, H.-G. Living ring-opening polymerization of *L*-lactide catalyzed by red-Al. *Organometallics* **2004**, *23*, 1411–1415. [[CrossRef](#)]
57. Sheldrick, G.M. Crystal structure refinement with *SHELXL*. *Acta Crystallogr. C* **2015**, *71*, 3–8. [[CrossRef](#)]
58. Dolomanov, O.V.; Bourhis, L.J.; Gildea, R.J.; Howard, J.A.K.; Puschmann, H. *OLEX2*: A complete structure solution, refinement and analysis program. *J. Appl. Cryst.* **2009**, *42*, 339–341. [[CrossRef](#)]